

Luis Montiel Campanón

**SYNTHESIS AND CHARACTERISATION OF $\{\text{Co}^{\text{III}}_2\text{Dy}^{\text{III}}_2\}$ AND $\{\text{V}^{\text{III}}_2\text{Dy}^{\text{III}}_2\}$
SINGLE MOLECULE MAGNETS**

FINAL DEGREE PROJECT

Directed by Dr Sophie Benjamin

Degree in Chemistry



UNIVERSITAT ROVIRA I VIRGILI

Tarragona

2017

Acknowledgements

I would like to express my sincere thanks to all those people who have contributed to the realization of this project.

Firstly, I would like to express my gratitude to my project tutor from Nottingham Trent University, Sophie Benjamin, for the help and the predisposition to progress with the project.

As for the people I met in Nottingham, I specially thank the PhD students Myles Terrey, Ryan Hemming and Jonathan Bristow, with whom I shared an important part of the time working in the laboratories and who created a very pleasant working environment. I also must mention all the Erasmus students I met in Nottingham as well, with whom I shared unforgettable experiences.

Last but by no means least, I really appreciate the unconditional support of my family, who is always there in spite of the distance.

Index

1. Abstract.....	4
2. Objective.....	4
3. Introduction.....	5
3.1 Historical context	6
3.2 Current challenges	9
3.3 The project	9
4. Basics of Single Molecule Magnet behaviour.....	9
4.1 Fundamental considerations	10
4.2 Magnetic measurements	12
5. Single crystal growth	13
5.1 X-ray diffraction	13
5.2 Crystal growth techniques	14
6. Experimental Section.....	17
6.1 Reagents and hazard and precautionary statements.....	17
6.2 Description of the experiments	22
7. Results and discussion	27
7.1 Butterfly {Co ^{III} ₂ Dy ^{III} ₂ } complexes	27
7.2 Butterfly {V ^{III} ₂ Dy ^{III} ₂ } complexes	37
8. Conclusions.....	41
9. References	42
10. Annexes	45

1. Abstract

Single Molecule Magnets (SMMs) are magnetic materials where the magnetic domains comprise individual molecules. This feature can lead to the development of applications related to high-density digital information storage.

In this project, new tetranuclear *butterfly complexes* $[TM^{III}_2Dy^{III}_2(\mu_3-OMe)_2(\text{amino-polyalcohol})_2(\text{carboxylic acid})_4(\text{MeOH})_4](NO_3)_2$ {TM = Co and V} have been tried to synthesize utilizing different amino-polyalcohols and carboxylic acids as bridging ligands. These complexes, which may display SMM behaviour, have been characterized by single crystal X-Ray diffraction, when possible, and IR spectroscopy. $[Co^{III}_2Dy^{III}_2(\mu_3-OMe)_2(BDEA^*)_2(O_2CPh)_4(\text{MeOH})_4](NO_3)_2$ is the only complex which has been able to crystallize as single crystals and further characterisation of the molecule has been carried out. As for the other butterfly complexes, the synthesis of main $\{Co^{III}_2Dy^{III}_2\}$ complexes have been verified by IR spectroscopy, while none of $\{V^{III}_2Dy^{III}_2\}$ complexes have been successfully synthesized.

*BDEA= doubly deprotonated N-Buthyldiethanolamine

2. Objective

This project consists in the synthesis and characterisation of new heterometallic 3d/4f *butterfly complexes* which may display SMM behaviour. Specifically, the aim of the project is the synthesis of $\{Co^{III}_2Dy^{III}_2\}$ and $\{V^{III}_2Dy^{III}_2\}$ tetranuclear butterfly complexes using amino-polyalcohols and carboxylic acids ligands. In collaboration with Dr. Stuart Langley at Manchester Metropolitan University, the magnetic properties of these complexes will be investigated.

3. Introduction

A traditional macroscopic magnet is composed of magnetic domains, three-dimensional regions of the material within which the spins are aligned (and which contain many atoms or molecules), between which there are domain walls. Hysteresis is observed in magnetisation vs field (M vs H) plots because altering the magnetisation requires the breaking of domain walls, which has an associated energy-cost. Thus, the magnetisation can be retained for a long time after removal of the field because the domains persist.¹

In Single Molecule Magnets (SMMs), the magnetic domains do not comprise many molecules, rather they comprise individual molecules and are magnetically isolated and are not interacting. SMMs therefore exhibit the properties associated with traditional macroscopic magnets, specifically retention of magnetisation and thus hysteresis in M vs H plots, but on a molecular scale, and to date only at very low temperatures¹.

Since SMMs can be considered as molecular analogues of classical bulk magnets, it was realized it might be possible to develop them for new technological applications involving the storage and processing of digital information. In contrast to bulk magnets currently used for this purpose, the molecular nature of SMMs offers unique attributes that may allow information to be stored with much higher densities, and to be processed at unprecedented speeds³. Therefore, this has involved looking at the potential of SMMs to fulfil applications in areas such as quantum computing or spintronic devices⁴. The scale of the advance can be seen by considering a typical magnetic tape which might store 90 minutes of music; if this tape was made of a material which displays SMM behaviour, the tape could store 150 years of music⁵.



Domains before magnetisation



Domains after magnetisation

Figure 1. In a material that is not magnetized, the magnetic domains point in random directions. In a magnetized material, all or most of the magnetic domains are arranged in the same direction. The image has been taken from the literature.²

3.1 Historical context

In the early 1990s, great excitement followed the discovery that a molecular transition metal coordination compound could, at liquid-helium temperatures, retain magnetization for long periods of time in the absence of an external magnetic field. The famous dodecametallic manganese-acetate cage $[\text{Mn}_{12}\text{O}_{12}(\text{OAc})_{16}(\text{H}_2\text{O})_4]$ (also known as $\{\text{Mn}_{12}\}$), as shown in **Figure 2**, became the progenitor of a large family of magnetic materials known as Single Molecule Magnets (SMMs).³

In the more than two decades since then, hundreds of SMMs have been reported and the field has become a prominent multi-disciplinary area of research, involving chemists, physicists and theoreticians in a combination of synthesis, structure determination, magneto-chemistry, spintronics and modelling.¹

The initial study focused in coordination complexes based on 3d metals, which led to the first generation of SMMs, highlighting $\{\text{Mn}_{12}\}$, the first SMM synthesized; Mn_{84} , the largest Mn cluster; $\{\text{Mn}_6\}$, transition metal-SMM which presents the largest *energy barrier* (See in section 4.1); $\{\text{Fe}\}$, the first mononuclear TM-SMM and $\{\text{Co}\}$, mononuclear Co^{II} transition metal-SMM. The structure of some of the most important transition metal-SMMs is shown in **Figure 3**.

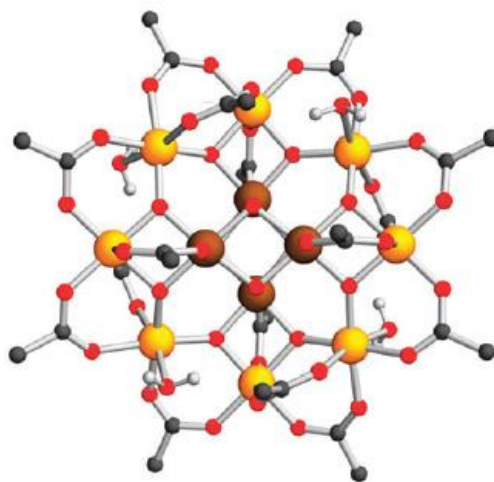


Figure 2. Molecular structure of $[\text{Mn}_{12}\text{O}_{12}(\text{OAc})_{16}(\text{H}_2\text{O})_4]$ cluster. Colour scheme: Mn^{III} : Orange; Mn^{IV} : brown; O: red; C: grey; H: white. All hydrogen atoms are omitted, except for those belonging to water molecules. The image has been taken from the literature.⁶

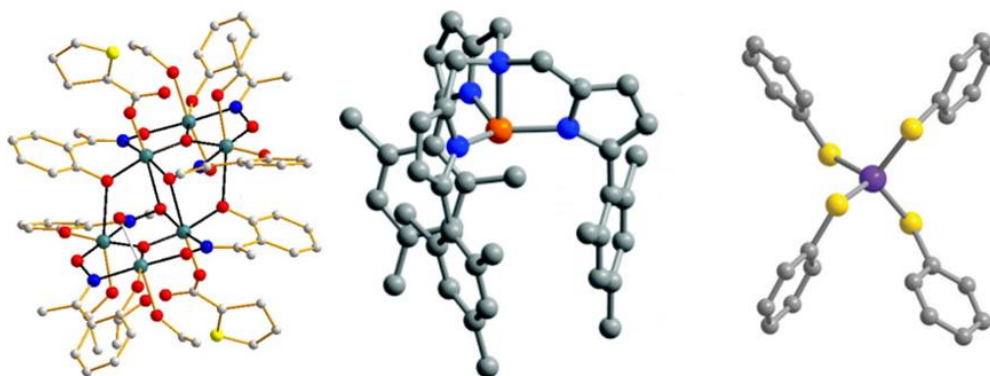


Figure 3. Structures of main transition metal-SMMs: $\{Mn_6\}$ or $[Mn^{III}_6O_2(MeSao)_6(O_2C\text{-thiophene})_2(EtOH)_4]$ (left), the core of Mn_6 is emphasized by black line. $\{Fe\}$ or $[Fe^{II}(tpa^{Mes})]$ (middle). $\{Co\}$ or $[Co^{II}(SPh)_4]^{2-}$ (right). Colour scheme: Mn: Green; Fe: orange; Co: purple; N: blue; O: red; S: yellow C: light grey. H-atoms are omitted for clarity. MeSao= 1-(2-hydroxyphenyl)ethanone oxime. tpa^{Mes} = Tris((5-mesityl-1H-pyrrol-2-yl)methyl)amine. Images have been taken from the literature.^{7,8,9}

Recently, particular emphasis has been placed on the design of new SMMs applying 4f metal ions leading to the second generation of SMMs, as a result of their significant *magnetic anisotropy* (see in section 4.1). Especially, Dy^{III} ion ($4f^9$) represents a very ideal ion because, as a number of the late lanthanides ($4f^n$, $n > 7$), it can provide stronger magnetic anisotropy than the early lanthanides ($n < 7$)¹⁰. Moreover, combination of both d-block and 4f elements into one molecule has been proven to be synergistic, making use of the magnetic properties of both metals.¹ Research into heterometallic 3d/4f complexes has also led to a flood of intriguing SMMs, emphasising the appearance in the last years of *butterfly complexes*.

In a 3d/4f heterometallic butterfly complex, the 4f ions are found in the central body positions and the trivalent 3d ions occupying the outer wing positions¹¹, as shown in **Figure 4**. Many compounds belonging to this family of complexes have been proven to display SMM behaviour, with large *anisotropic barriers* and slow *relaxation times*¹² (see in section 4.1).

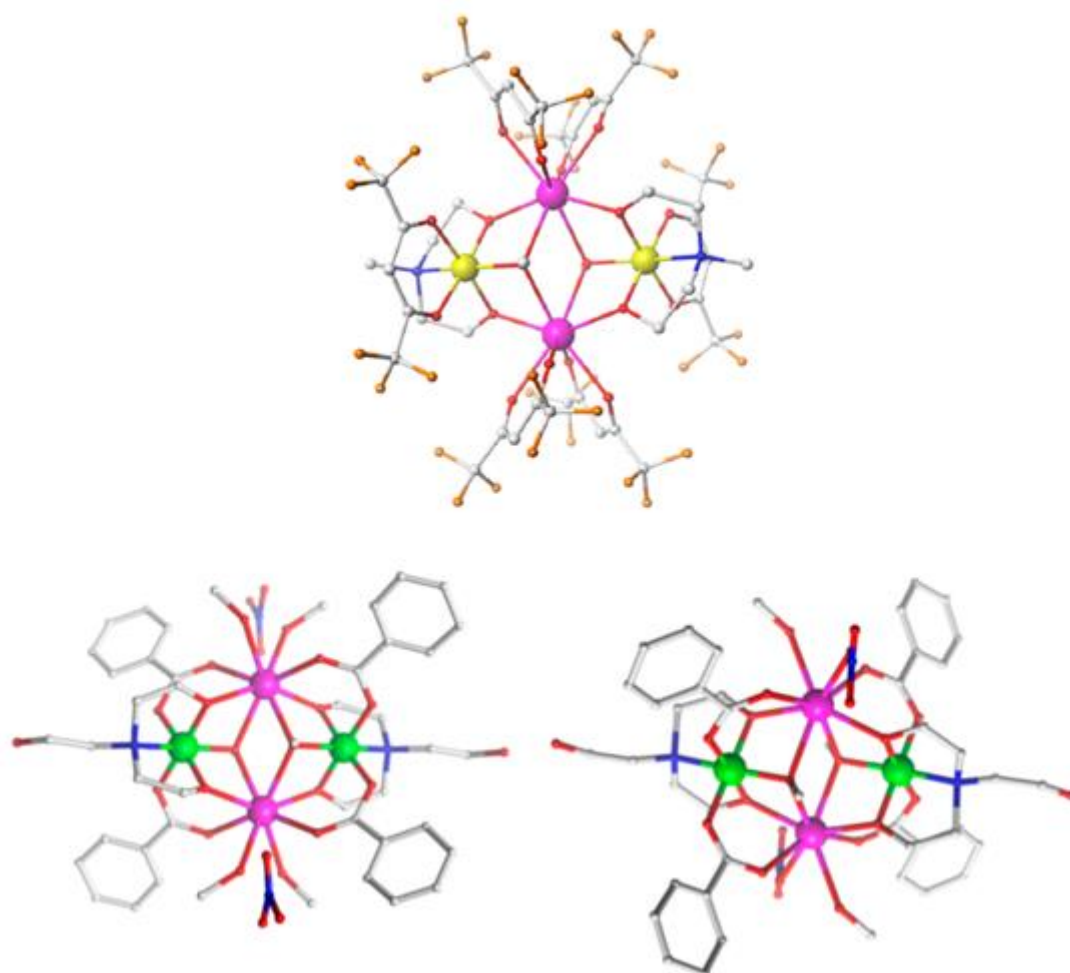


Figure 4. Structures of $\{TM^{III}Dy^{III}\}$ butterfly complexes (TM= Cr and Co). $[Cr_2^{III}Dy_2^{III}(OMe)_2(mdea)_2(hfacac)_6]$ (above). $[Dy_2^{III}Co_2^{III}(OMe)_2(teaH)_2(O_2CPh)_4(MeOH)_4](NO_3)_2 \cdot MeOH \cdot H_2O$ (bottom on the left) and $[Dy_2^{III}Co_2^{III}(OMe)_2(teaH)_2(O_2CPh)_4(MeOH)_2(NO_3)_2] \cdot MeOH \cdot H_2O$ (bottom on the right) are found to cocrystallise in the same crystal. Solvent and H-atoms are omitted for clarity. Colour scheme: Co^{III} : green; Cr^{III} : yellow; Dy^{III} : purple; F: orange; O: red; N: blue; C: light grey. mdea= N-methyldiethanolamine. hfacac = hexafluoroacetylacetonate. $teaH^{2-}$ = doubly deprotonated triethanolamine. Images have been taken from the literature.^{11,12}

3.2 Current challenges

One of the grand challenges in this field is still to design and to synthesize efficient SMMs that function at temperatures likely to be of practical use. Currently, the unique properties of SMMs are only accessible using liquid helium cooling, therefore, either the operating temperatures need to rise significantly, or applications so novel and important need to be discovered that temperature ceases to be an issue³.

Whilst at present this seems a massive challenge, researchers in the superconductivity field faced a similarly challenging situation, and did make a huge step up in critical temperature, from liquid helium to liquid nitrogen temperatures, and superconducting materials are now used in a wide range of commercial applications¹.

3.3 The project

Encouraged by the current challenge, the synthesis and characterisation of new heterometallic 3d/4f butterfly complexes which may display SMM behaviour has been performed. The project was carried out in the laboratories of the School of Science and Technology of Nottingham Trent University (England) from February 2017 to May 2017 and research has been supervised by Dr Sophie Benjamin.

Before this investigation, some $\{\text{Co}^{\text{III}}_2\text{Dy}^{\text{III}}_2\}$ butterfly complexes had already been reported^{4,12,13} while $\{\text{V}^{\text{III}}_2\text{Dy}^{\text{III}}_2\}$ butterfly complexes had not.

4. Basics of Single Molecule Magnet behaviour

Theoretical basis of Single Molecule Magnets is provided below for a more accurate comprehension of SMM operation.

4.1 Fundamental considerations

Single Molecule Magnets are individual molecules which have a significant *energy barrier* (U) to a change in orientation of their molecular spin. This property allows the orientation of the spin to be maintained below a *blocking temperature* (T_B) upon application and removal of a magnetic field, thus allowing digital information to be stored on a single molecule.

To display SMM behaviour, a complex must have a non-zero total ground spin state, S . Furthermore, molecules need to be well isolated in the solid state, otherwise bulk magnetic behaviour may be observed. This is usually achieved by the use of ligands with bulky organic peripheries, thus many SMMs present complex structures¹.

The origin of the barrier lies in the magnetic anisotropy associated with the 3d and 4f metal ions found in the structures of SMMs.¹ The anisotropy of the magnetisation is the result of *zero field splitting* (ZFS), which is quantified by the parameter D . ZFS lifts the degeneracy of the $2S+1$ M_S spin states of a complex due to magnetic dipolar interactions between unpaired electrons and interactions with excited states via spin-orbit coupling⁵. The effect of ZFS is fairly well understood in 3d complexes, but less so for 4f complexes¹, so the explanation is focused on the former.

In a complex with a total spin S there are $2S + 1$ possible spin states, each sublevel described by a spin quantum number M_S . The M_S quantum number depends on S and ranges in value from S to $-S$ in

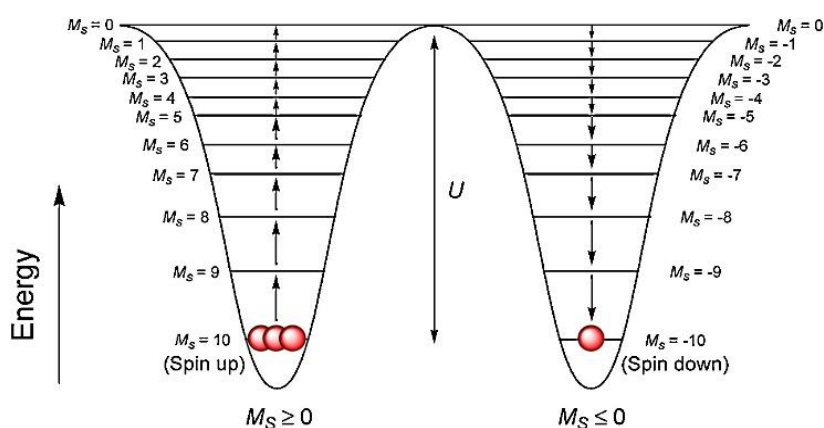


Figure 5. Schematic representation of the splitting of the $S = 10$ ground state of $\{Mn_{12}\}$ into 21 sublevels by ZFS. This image has been taken from literature.¹

increments of one. The degeneracy of the $2s + 1$ M_S spin states can be lifted via ZFS, as shown in **Figure 5**. The form of the ZFS depends on the symmetry of the molecule.

Hence, ZFS may arise if the symmetry of the SMM is lower than cubic. If no anisotropy is present, the M_S states all have the same energy.¹⁴

Each M_S state corresponds to a different orientation of the spin projection, and $M_S = S$ can be considered *spin up* and $M_S = -S$ *spin down* (**Figures. 5 and 6**) or 1 and 0 in binary coding, respectively. M_S states split in zero field according to **Eq. 1**. Therefore, when D is negative, $M_S = \pm S$ become lower in energy than the intermediary sublevels M_S with $S > M_S > -S$ ¹, as shown in **Figures 5 and 6**.

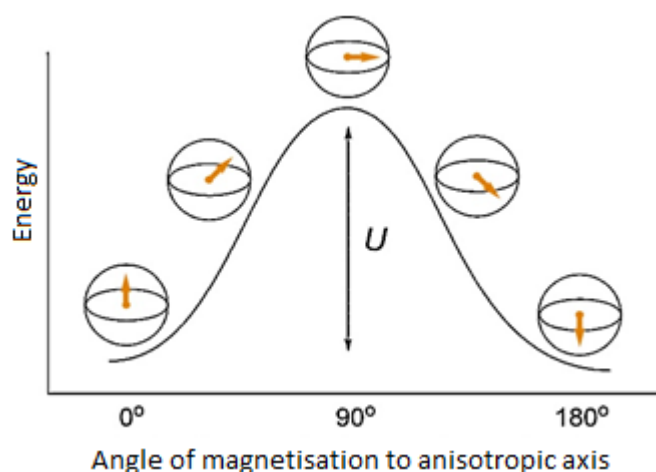


Figure 6. Energetic preference of the spin projection in an SMM. The energetically most favourable direction for the spin projection is called anisotropic axis. This image has been taken from literature.¹

$$E(M_S) \propto D \cdot M_S^2 \quad (\text{Eq. 1})$$

The size of the energy barrier to spin reversal is related to both D and S according to **Eq.2**.

$$U = |D| \cdot S^2 \quad (\text{Eq. 2})$$

The energetically most favourable direction for the spin projection is called *anisotropic axis* or *easy axis*. Hence, to magnetize a SMM the magnetic field is applied through the easy axis to lower the energy of one well and to increase the energy of the other. Therefore, in a magnetic field the equilibrium now favours the orientation of the spin aligned with the magnetic field and magnetisation of the SMM occurs, as shown in **Figure 7**.

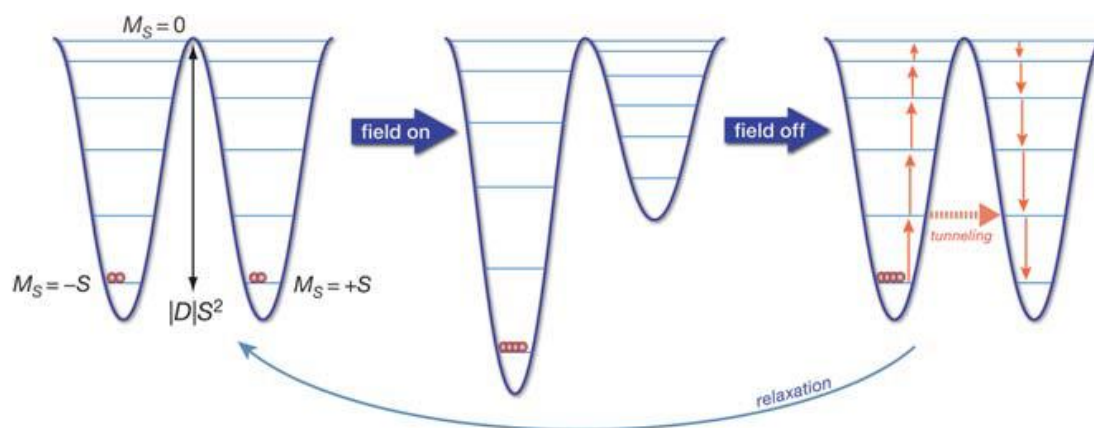


Figure 7. Spin down is stabilized under the applied magnetic field and, after removal of the field and at sufficiently low temperatures, magnetisation persists because there is insufficient thermal energy to make some of the particles jump over the barrier and reverse their magnetisation. This image has been taken from the literature.¹⁵

However, if the particles are given enough time, half of them will be in the left well and half in the right well at equilibrium because the two minima have the same energy. The system will no longer be magnetized in zero magnetic field and this process is called *relaxation of magnetization*, which can also be promoted by quantum tunnelling.¹⁶

4.2 Magnetic measurements

The success (or not) of an SMM can be measured by the magnetic blocking temperature (T_B) which is the highest temperature at which an SMM displays hysteresis in plots of magnetization (M) versus magnetic field (H) (**Figure 8**). Gatteschi, Villain, and Sessoli have proposed T_B as being the temperature at which the time (τ) taken for the magnetization to relax is 100 seconds.³ Therefore, the larger the energy barrier to spin reversal (U), the longer magnetisation can be retained and the higher the temperature this can be observed at.¹

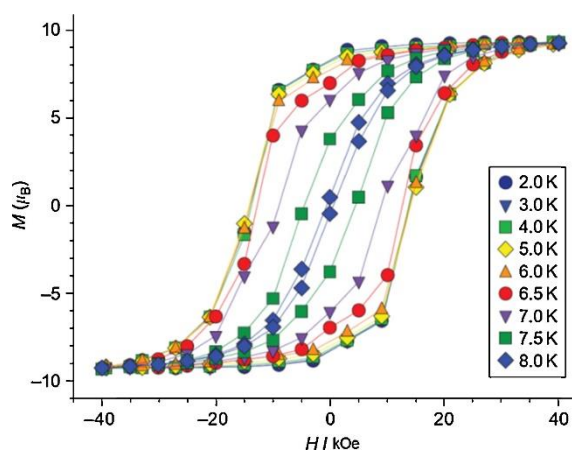


Figure 8. Hysteresis in the field dependence of magnetisation at different temperatures at a fast average sweep rate of $800 \text{ Oe}\cdot\text{s}^{-1}$ ($0.08 \text{ T}\cdot\text{s}^{-1}$) for $[\text{K}(\text{18-crown-6})][\{(\text{Me}_3\text{Si})_2\text{N}\}_2\text{Dy}^{\text{III}}(\text{THF})_2\}]$. This SMM presents one of the highest T_B values observed to date (8,3 K). This image has been taken from the literature.¹⁷

The relationship between the barrier to relaxation of the magnetisation and the ground spin state S led to a vast effort towards building the compounds with the highest possible nuclearity, in an attempt to maximise U . However, it was found the anisotropy constant D to be inversely proportional to S^2 . Therefore, incorporating large numbers of paramagnetic transition metal ions in a compound may be antagonistic to generating a large magnetic anisotropy.¹⁴

The bottom line in all of this is that a good SMM needs a large thermal barrier (U) and no (or slow) quantum tunnelling of magnetisation (QTM), so that the blocking temperature (T_B) is as high as possible¹.

5. Single crystal growth

In this section a description of X-ray diffraction, the main technique used to characterize the products in this project, and different crystallization techniques carried out during the research are explained. Hence, a more accurate comprehension is provided before the explanation of the Experimental Part in section 5.

5.1 X-ray diffraction

As the expected products in this project are supposed to be paramagnetic, nuclear magnetic resonance (NMR), one of the most powerful characterization techniques, cannot easily be used to characterize them. Therefore, crystal growth was carried out to characterize the tetranuclear $\{\text{Co}^{\text{III}}_2\text{Dy}^{\text{III}}_2\}$ and $\{\text{V}^{\text{III}}_2\text{Dy}^{\text{III}}_2\}$ complexes by single crystal X-ray diffraction.

Single crystal X-ray diffraction (XRD) is a crystallographic method for determining atomic structures (an X-ray diffractometer is shown in **Figure 9**). A beam of X-rays strikes a crystal and is diffracted. From the angles and intensities of the diffracted rays, a 3D map of electron density of the crystal can be constructed and the arrangement of atoms and bonds within the crystal can be inferred. This technique is one of the least ambiguous and most complete ways of characterizing a compound. In order to take advantage of these benefits, the compound in question has to be rendered as a crystal of suitable size and quality.¹⁸



Figure 9. Single crystal X-ray diffractometer. A crystal is mounted and displayed in the screen placed at the top right. Image has been taken from the literature.¹⁹

The most promising crystals for XRD are transparent and have sharp edges.¹⁸ For diffraction work, the object is to obtain a small number of crystals with the mentioned features. As long as this is achieved, yield is irrelevant and purity is likely to be enhanced. To this end, crystals should be grown slowly, taking from minutes to months depending on the system. To understand why this is important, the process of growth at a crystal surface must be visualized: the greater the rate at which molecules arrive at the surface, the less time they have to orient themselves in relation to molecules already there and random accretion is more likely, leading to crystals which are twinned or disordered. Suitable growth conditions include the absence of dust and vibration: if these are present they can lead to crystals which are small or non-singular.²⁰

5.2 Crystal growth techniques

Each technique for growing crystals relies on creating a situation where the solute can no longer dissolve in the solvent. This usually involves preparing a saturated solution then altering the conditions, such as temperature and volume of solvent, so that the solvent is unable to contain the material in it. If the change is slow enough, the solute molecules have time to arrange themselves and pack closely, creating a well-defined crystal.²¹

Different crystal growth techniques were carried out throughout the project in order to obtain the best possible crystals. Furthermore, many of them had to be adapted for use with air-sensitive compounds due to V^{III} willingness to oxidize into V^{IV} and V^V compounds under aerobic conditions. Therefore, working under inert atmosphere was required and such conditions demand the use of Schlenk flasks and the Schlenk line to carry out the reactions under N_2 atmosphere.

The Schlenk line consists of two manifolds, as shown in **Figure 10**, one attached to a vacuum pump and the other to a source of inert gas. It allows Schlenk flasks to be evacuated of air and moisture and refilled with the inert gas via the side arm of the flask. The side arm is fitted with a ground glass stopcock which allows the flask to be isolated from the atmosphere.²²

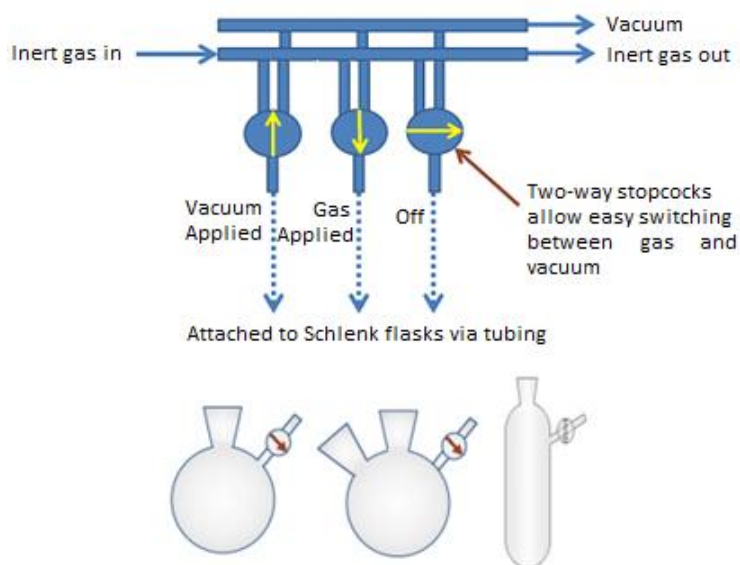


Figure 10. Basic Schlenk line and types of Schlenk flask available. Image has been taken from the literature.²²

Four main crystal growth techniques were carried out during the project, which are described below:

- **Slow evaporation:** this is one of the simplest methods and is generally the first attempted. It is only suitable for compounds that are air and moisture stable at room temperature. It involves the slow evaporation of the solvent from the solution containing the compound until saturation is reached and crystals begin to form.

- **Cooling:** The technique involves cooling a saturated solution. As the temperature drops, the solvent's ability to dissolve the solute decreases and excess solute precipitates out. If the rate of cooling is slow enough, crystals should form.
- **Liquid/Liquid diffusion or layering technique:** This technique involves the slow diffusion of one solvent into another. Two solvents are added to a vessel so that they form distinct layers (**Figure 11**). A solvent in which the compound is moderately soluble is chosen as the first solvent and forms the bottom layer. A less dense solvent, in which the compound is insoluble, is chosen as the second solvent and forms the top layer. Solvent 2 gradually diffuses into solvent 1, creating a solvent mixture with lower solubility for the compound than that of pure solvent 1. As solvent 2 increasingly diffuses into solvent 1, the solubility decreases more and more, forcing the product to precipitate, which may form crystals at the liquid/liquid boundary.

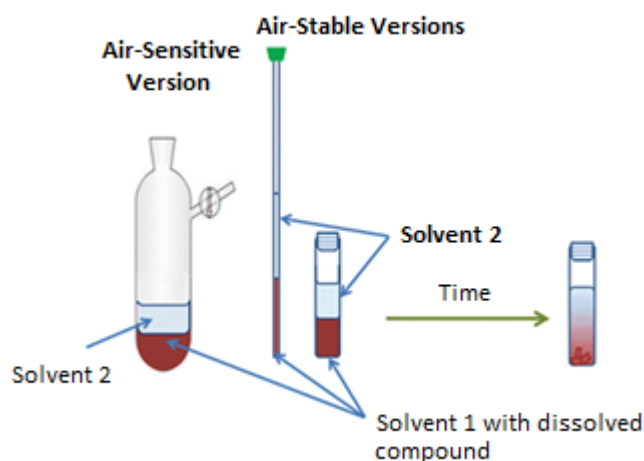


Figure 11. The liquid/liquid diffusion or layering technique for growing crystals. Image has been taken from the literature.²²

- **Vapour Diffusion:** This technique involves the diffusion of the vapor of a volatile solvent, in which the compound is not soluble, into the solvent containing the sample to be crystallized (**Figure 12**). The theory behind it is similar to that of the layering and is considered as a *slow layering*. The advantages of this method include the relatively slow rate of diffusion, its controllability and its adaptability, for

example in combination with Schlenk techniques to grow crystals of air-sensitive samples.²⁰

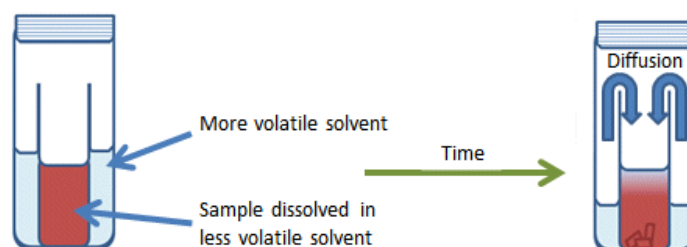


Figure 12. Vapour diffusion technique for air stable compounds. Image has been taken from the literature.²²

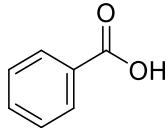
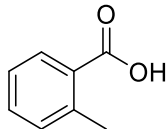
In the Experimental Section not all the explained crystal growth techniques appear since just those procedures which provided better results are explained. However, before reaching the explained procedure, in many cases the other crystal growth techniques were tested.

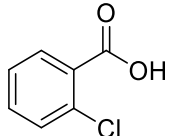
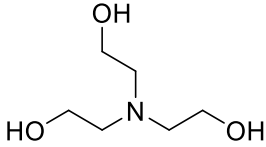
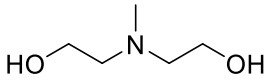
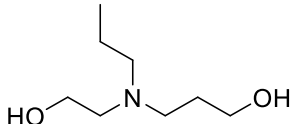
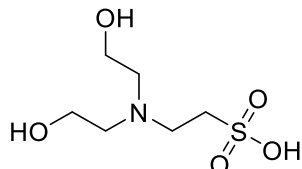
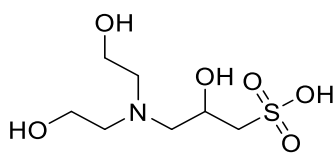
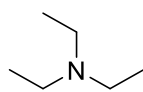
6. Experimental Section

6.1 Reagents and hazard and precautionary statements

Main reagents with their purity and chemical formula are listed in **Table 1** in conjunction with **Table 2** which shows hazard and precautionary statements of these reagents. All chemicals and solvents were obtained from commercial sources.

Table 1. List of the main reagents used during the project.

Reagent	Purity	Formula
Acetonitrile anhydrous	99,8%	$\text{N}\equiv\text{C}-\text{CH}_3$
Methanol anhydrous	99,8%	CH_3-OH
Cobalt (II) nitrate hexahydrate	98,0-102,0%	$\text{Co}(\text{NO}_3)_2 \cdot 6\text{H}_2\text{O}$
Cobalt (II) chloride hexahydrate	99,999%	$\text{CoCl}_2 \cdot 6\text{H}_2\text{O}$
Dysprosium (III)nitrate hydrate	99,9%	$\text{Dy}(\text{NO}_3)_3 \cdot \text{XH}_2\text{O}$
Vanadium (III) chloride	97%	VCl_3
Trichlorotris(tetrahydrofuran)vanadium	_*	$\text{VCl}_3 \cdot 3\text{THF}$
Benzoic acid	$\geq 99,5\%$	
o-Toluic acid	99%	

2-Chlorobenzoic acid	98%	
Triethanolamine	≥98%	
N-Methyldiethanolamine (MDEA)	≥99%	
N-Butyldiethanolamine (BDEA)	≥98,6%	
N,N-Bis(2-hydroxyethyl)-2-aminoethanesulfonic acid (BES)	≥99%	
N,N-Bis(2-hydroxyethyl)-3-amino-2-hydroxypropanesulfonic acid (DISPO)	97%	
Triethylamine	≥99%	
Sodium methoxide	95%	$\text{Na}^+ \text{ } ^-\text{O}$

*Trichlorotris(tetrahydrofuran)vanadium was synthesized from commercial VCl_3 and commercial tetrahydrofuran in the laboratory and purity was not calculated.

Table 2. List of hazard and precautionary statements of the main reagents used during the project.

Reagent	Hazard and precautionary statements
Acetonitrile anhydrous	<p>Hazard statements</p> <ul style="list-style-type: none"> • Highly flammable liquid and vapour. • Harmful if swallowed, in contact with skin or if inhaled. • Causes serious eye irritation. <p>Precautionary statements</p> <ul style="list-style-type: none"> • Keep away from heat, hot surfaces, sparks, open flames and other ignition sources. No smoking. • Wear protective gloves/ protective clothing.
Methanol anhydrous	<p>Hazard statements</p> <ul style="list-style-type: none"> • Highly flammable liquid and vapour. • Harmful if swallowed and in contact with skin. <p>Precautionary statements</p> <ul style="list-style-type: none"> • Keep away from heat, hot surfaces, sparks, open flames and other ignition sources. No smoking. • Wear protective gloves/ protective clothing.
Cobalt (II) nitrate hexahydrate	<p>Hazard statements</p> <ul style="list-style-type: none"> • May intensify fire; oxidiser. • Very toxic to aquatic life with long lasting effects. <p>Precautionary statements</p> <ul style="list-style-type: none"> • Avoid breathing dust/ fume/ gas/ mist/ vapours/ spray. • Wear protective gloves/ protective clothing/ eye protection/ face protection.
Dysprosium (III)nitrate hydrate	<p>Hazard statements</p> <ul style="list-style-type: none"> • May intensify fire; oxidiser. • Causes skin, eye and respiratory irritation. <p>Precautionary statements</p> <ul style="list-style-type: none"> • Keep/Store away from clothing/ combustible materials. • Avoid breathing dust/ fume/ gas/ vapours/ spray.
Vanadium (III) chloride	<p>Hazard statements</p> <ul style="list-style-type: none"> • Harmful if swallowed. • Causes severe skin burns and eye damage. <p>Precautionary statements</p> <ul style="list-style-type: none"> • Wear protective gloves/ protective clothing/ eye protection/ face protection.
Trichlorotris(tetrahydrofuran) vanadium	<p>Hazard statements</p> <ul style="list-style-type: none"> • Flammable solid. • Harmful if swallowed and in contact with skin.

	<p>Precautionary statements</p> <ul style="list-style-type: none"> Keep away from heat, hot surfaces, sparks, open flames and other ignition sources. No smoking.
Benzoic acid o-Toluic acid 2-Clorobenzoic acid	<p>Hazard statements</p> <ul style="list-style-type: none"> Causes skin irritation and eye damage. May cause respiratory irritation. <p>Precautionary statements</p> <ul style="list-style-type: none"> Avoid breathing dust/fume/gas/vapours/ spray. Wear protective gloves/eye protection/face protection.
Triethanolamine	<p>Hazard statements</p> <ul style="list-style-type: none"> Non-hazardous substance <p>Precautionary statements</p> <ul style="list-style-type: none"> None listed. Wear PPE as a precaution.
N-Methyldiethanolamine (MDEA) N-Buthyldiethanolamine (BDEA)	<p>Hazard statements</p> <ul style="list-style-type: none"> Causes severe skin burns and eye damage. <p>Precautionary statements</p> <ul style="list-style-type: none"> Wear protective gloves/protective clothing/eye protection/ face protection.
N,N-Bis(2-hydroxyethyl)-2-aminoethanesulfonic acid (BES)	<p>Hazard statements</p> <ul style="list-style-type: none"> Causes skin and eye irritation. May cause respiratory irritation <p>Precautionary statements</p> <ul style="list-style-type: none"> Avoid breathing dust.
N,N-Bis(2-hydroxyethyl)-3-amino-2-hydroxypropanesulfonic acid (DISPO)	<p>Hazard statements</p> <ul style="list-style-type: none"> Non-hazardous substance <p>Precautionary statements</p> <ul style="list-style-type: none"> None listed. Wear Personal Protective Equipment (PPE) as a precaution.
Triethylamine	<p>Hazard statements</p> <ul style="list-style-type: none"> Highly flammable liquid and vapour. Toxic in contact with skin and if inhaled. <p>Precautionary statements</p> <ul style="list-style-type: none"> Keep away from heat/sparks/open flames. Wear protective gloves/protective clothing/eye protection/face protection.
Sodium methoxide	<p>Hazard statements</p> <ul style="list-style-type: none"> Self-heating: may catch fire. Causes severe skin burns and eye damage. <p>Precautionary statements</p> <ul style="list-style-type: none"> Protect from sunlight. Wear protective gloves/protective clothing/eye protection/face protection.

6.2 Description of the experiments

The synthesis of $\{\text{Co}^{\text{III}}_2\text{Dy}^{\text{III}}_2\}$ and $\{\text{V}^{\text{III}}_2\text{Dy}^{\text{III}}_2\}$ tetranuclear butterfly complexes was carried out using two families of polydentate ligands:

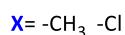
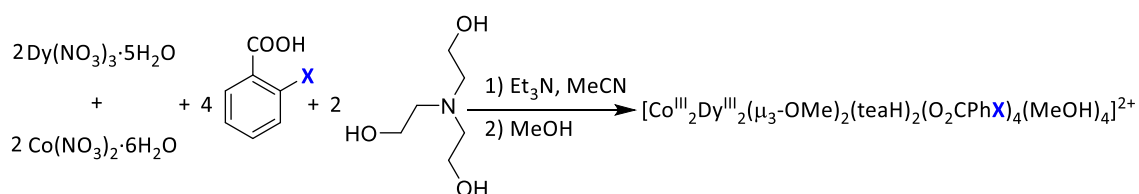
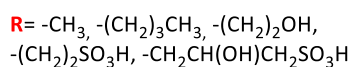
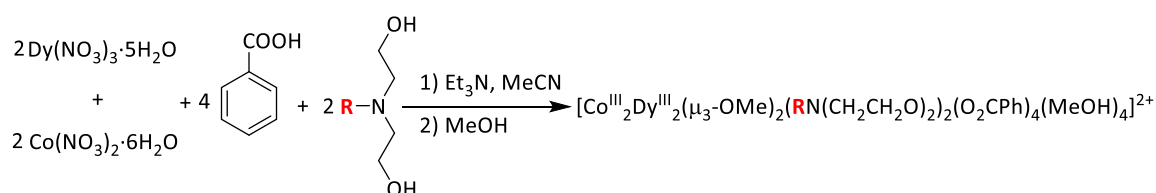
- Amino-polyalcohols: TEA, MDEA, BDEA, BES and DIPSO
- Benzoic acid and derivatives: benzoic acid, o-toluic acid and 2-chlorobenzoic acid

 Synthesis of butterfly $\{\text{Co}^{\text{III}}_2\text{Dy}^{\text{III}}_2\}$ complexes

The synthetic strategy focused on synthesizing tetranuclear $\{\text{Co}^{\text{III}}_2\text{Dy}^{\text{III}}_2\}$ complexes using the two families of polydentate ligands as follows:

- Using different amino-polyalcohol ligands and benzoic acid.
- Using different benzoic acid derivatives and triethanolamine (TEA).

All reactions were carried out under aerobic conditions. Under these conditions Co^{II} oxidized into Co^{III} . **Scheme 1** shows the followed synthetic strategy.



Scheme 1. Reaction scheme of the synthesis of butterfly $\{\text{Co}^{\text{III}}_2\text{Dy}^{\text{III}}_2\}$ complexes. According to the literature¹² the product may have various combinations of MeOH and NO_3^{2-} ligands, e.g., $(\text{MeOH})_4$ (cationic complex) or $(\text{MeOH})_2(\text{NO}_3)_2$ (neutral complex).

Synthesis of $[\text{Co}^{\text{III}}_2\text{Dy}^{\text{III}}_2(\mu_3\text{-OMe})_2(\text{teaH})_2(\text{O}_2\text{CPh})_4(\text{MeOH})_2](\text{NO}_3)_2 \cdot \text{MeOH} \cdot \text{H}_2\text{O}$ (1a**) and $[\text{Co}^{\text{III}}_2\text{Dy}^{\text{III}}_2(\mu_3\text{-OMe})_2(\text{teaH})_2(\text{O}_2\text{CPh})_4(\text{MeOH})_4](\text{NO}_3)_2 \cdot \text{MeOH} \cdot \text{H}_2\text{O}$ (**1b**).** $\text{Co}(\text{NO}_3)_2 \cdot 6\text{H}_2\text{O}$ (0.15 g, 0.5 mmol) and $\text{Dy}(\text{NO}_3)_3 \cdot 5\text{H}_2\text{O}$ (0.22 g, 0.5 mmol) were dissolved in MeCN (15 ml), followed by addition of triethanolamine (teaH_3) (0.07 ml, 0.5 mmol), benzoic acid (0.12 g, 1 mmol), and triethylamine (0.35 ml, 2.5 mmol) to give a purple solution. This was stirred for 6 h, after which the MeCN was removed and the residue redissolved in MeOH (10ml), which was allowed to stand. Within 2-3 days blue/purple needles of **1** (**1a** and **1b**) had crystallized. Crystals were filtered by vacuum filtration and cleaned with some ml of Et_2O . The approximate yield was 56%

The same experiment was carried out using $\text{CoCl}_2 \cdot 6\text{H}_2\text{O}$ (0.12 g, 0.5 mmol) instead of $\text{Co}(\text{NO}_3)_2 \cdot 6\text{H}_2\text{O}$ as cobalt source and **1** was obtained in an approximate yield of 20%.

Synthesis of $[\text{Co}^{\text{III}}_2\text{Dy}^{\text{III}}_2(\mu_3\text{-OMe})_2(\text{bdea})_2(\text{O}_2\text{CPh})_4(\text{MeOH})_4](\text{NO}_3)_2$ (2**).** The same procedure was used to synthesize **2** except that N-butyldiethanolamine (bdeaH_2) (0.08 ml, 0.5 mmol) was used in place of triethanolamine (teaH_3). Within 2-3 days black needles of **2** had crystallized. Crystals were filtered by vacuum filtration and cleaned with some ml of Et_2O . The approximate yield was 23%.

Synthesis of $[\text{Co}^{\text{III}}_2\text{Dy}^{\text{III}}_2(\mu_3\text{-OMe})_2(\text{mdea})_2(\text{O}_2\text{CPh})_4(\text{MeOH})_4](\text{NO}_3)_2$ (3**).** The same procedure was used to synthesize **3** except that N-methyldiethanolamine (mdeaH_2) (0.06 ml, 0.5 mmol) was used in place of triethanolamine (teaH_3). Within 2-3 days grey powder of **3** appeared. Powder was filtered by vacuum filtration and cleaned with some ml of Et_2O . The approximate yield was 29%.

Synthesis of $[\text{Co}^{\text{III}}_2\text{Dy}^{\text{III}}_2(\mu_3\text{-OMe})_2(\text{besH})_2(\text{O}_2\text{CPh})_4(\text{MeOH})_4](\text{NO}_3)_2 \cdot \text{MeOH} \cdot \text{H}_2\text{O}$ (4**).** The same procedure was used to synthesize **4** except that N,N-bis(2-hydroxyethyl)-2-aminoethanesulfonic acid (besH_3) (0.11 g, 0.5 mmol) was used in place of triethanolamine (teaH_3). In this case, vapour diffusion was carried out for crystallization using 10 ml of Et_2O . Within 3 days pink powder of **4** appeared. Powder was filtered by vacuum filtration and cleaned with some ml of Et_2O . The approximate yield was 13%.

Synthesis of $[\text{Co}^{\text{III}}_2\text{Dy}^{\text{III}}_2(\mu_3\text{-OMe})_2(\text{dipsoH}_2)_2(\text{O}_2\text{CPh})_4(\text{MeOH})_4](\text{NO}_3)_2\cdot\text{MeOH}\cdot\text{H}_2\text{O}$ (5).

The same procedure was used to synthesize **5** except that N,N-bis(2-hydroxyethyl)-3-amino-2-hydroxypropanesulfonic acid (DIPSOH₄) (0.12 g, 0.5 mmol) was used in place of triethanolamine (teaH₃). Within 4-5 days red/purple microcrystalline powder of **5** had crystallized. Powder was filtered by vacuum filtration and cleaned with some ml of Et₂O. The approximate yield was 27%

Synthesis of $[\text{Co}^{\text{III}}_2\text{Dy}^{\text{III}}_2(\mu_3\text{-OMe})_2(\text{teaH})_2(\text{o-tol})_4(\text{MeOH})_4](\text{NO}_3)_2\cdot\text{MeOH}\cdot\text{H}_2\text{O}$ (6).

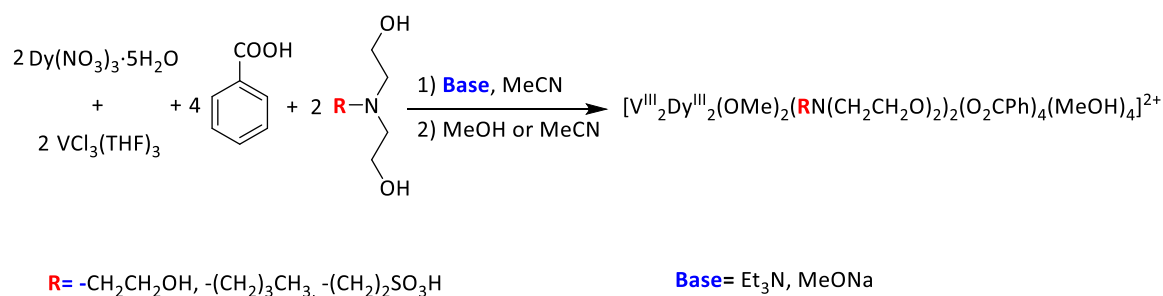
The same procedure was used to synthesize **6** except that o-toluic acid (o-tolH) (0.14 g, 1 mmol) was used in place of benzoic acid. In this case, within 5-6 days no crystals appeared. Once MeOH was removed, an oily black residue was obtained. The residue was cleaned with some ml of Et₂O and the obtained amount was 0.73 g. Yield was not calculated due to the likely presence of impurities.

Synthesis of $[\text{Co}^{\text{III}}_2\text{Dy}^{\text{III}}_2(\mu_3\text{-OMe})_2(\text{teaH})_2(\text{O}_2\text{CPh-2-Cl})_4(\text{MeOH})_4](\text{NO}_3)_2\cdot\text{MeOH}\cdot\text{H}_2\text{O}$ (7).

The same procedure was used to synthesize **7** except that 2-chlorobenzoic acid (HO₂CPh-2-Cl) (0.16 g, 1 mmol) was used in place of benzoic acid. Within 4-5 days dark purple powder of **7** had crystallized. Powder was filtered by vacuum filtration and cleaned with some ml of Et₂O. The approximate yield was 15%.

Synthesis of butterfly $\{\text{V}^{\text{III}}_2\text{Dy}^{\text{III}}_2\}$ complexes

The synthetic strategy focused on synthesizing tetranuclear $\{\text{V}^{\text{III}}_2\text{Dy}^{\text{III}}_2\}$ complexes using benzoic acid and different amino-polyalcohol ligands. All reaction procedures were carried out under anaerobic conditions to avoid V^{III} oxidation and solvents had to be dried and degassed before use. **Scheme 2** shows the followed synthetic strategy.



Scheme 2. Reaction scheme of the synthesis of butterfly $\{\text{V}^{\text{III}}_2\text{Dy}^{\text{III}}_2\}$ complexes. According to the literature¹² the product may have various combinations of MeOH and NO_3^{2-} ligands, e.g., $(\text{MeOH})_4$ (cationic complex) or $(\text{MeOH})_2(\text{NO}_3)_2$ (neutral complex).

Attempted synthesis of $[\text{V}^{\text{III}}_2\text{Dy}^{\text{III}}_2(\mu_3\text{-OMe})_2(\text{teaH})_2(\text{O}_2\text{CPh})_4(\text{MeOH})_4](\text{NO}_3)_2 \cdot (8)$.

$\text{Dy}(\text{NO}_3)_3 \cdot 5\text{H}_2\text{O}$ (0.22 g, 0.5 mmol), triethanolamine (teaH_3) (0.07 ml, 0.5 mmol), benzoic acid (0.12 g, 1 mmol) and sodium methoxide (0.14 g, 2.5 mmol) were placed in a Schlenk flask and dried under vacuum for 10 min. After that, reagents were dissolved in dry and degassed MeCN (10 ml) to give a white suspension. The suspension was degassed under N_2 flow for 30 min. $\text{VCl}_3 \cdot 3\text{THF}$ (0.19 g, 0.5 mmol) was dissolved in dry and degassed MeCN (5 ml) to give a green solution. $\text{VCl}_3 \cdot 3\text{THF}$ solution was added to the white ligands suspension and a pale green suspension was formed, which was stirred for 6h. After that time, a pale green solution was obtained, MeCN was removed and the residue redissolved in dried and degassed MeOH (10 ml). The solution was filtered by cannula and a brown solution was obtained. Vapor diffusion was carried out with Et_2O (10 ml) for crystallization. Within 4 days, colourless crystals had appeared. Crystallographic data verified crystals did not contain the desired butterfly complex but a chlorinated salt of protonated triethanolamine (teaH_4Cl). Therefore, the product reaction yield was 0% and the by-product reaction yield was approximately 67%.

Attempted synthesis of $[\text{V}^{\text{III}}_2\text{Dy}^{\text{III}}_2(\mu_3\text{-OMe})_2(\text{bdea})_2(\text{O}_2\text{CPh})_4(\text{MeOH})_4](\text{NO}_3)_2 \cdot (9)$.

$\text{Dy}(\text{NO}_3)_3 \cdot 5\text{H}_2\text{O}$ (0.22 g, 0.5 mmol), N-buthyldiethanolamine (bdeaH_2) (0.08 ml, 0.5 mmol) and benzoic acid (0.12 g, 1 mmol) were placed in a Schlenck flask and dried under vacuum for 10 min. Triethylamine (0.35 ml, 2.5 mmol) was then added and the reagents were dissolved in dry and degassed MeCN (10 ml). After that, the same procedure than that of **9** was followed. Within 4 days, yellow needles had crystallized. The solvent was removed via syringe and some ml of Et_2O were used to clean the product. Et_2O was also

removed via syringe and the product dried under vacuum. Crystallographic data verified crystals did not contain the desired butterfly complex but a non-reported coordination complex: $[\text{Dy}(\text{O}_2\text{CPh})_3(\text{MeOH})_2]$. Therefore, the product reaction yield was 0% and the by-product reaction yield was approximately 41%.

Attempted synthesis of $[\text{V}^{\text{III}}_2\text{Dy}^{\text{III}}_2(\mu_3\text{-OMe})_2(\text{besH})_2(\text{O}_2\text{CPh})_4(\text{MeOH})_4](\text{NO}_3)_2 \cdot (10)$.

$\text{Dy}(\text{NO}_3)_3 \cdot 5\text{H}_2\text{O}$ (0.22 g, 0.5 mmol), N,N-bis(2-hydroxyethyl)-2-aminoethanesulfonic acid (besH_3) (0.11 g, 0.5 mmol) and benzoic acid (0.12 g, 1 mmol) were placed in a Schlenk flask and dried under vacuum for 10 min. Triethylamine (0.35 ml, 2.5 mmol) was then added and the reagents were dissolved in dry and degassed MeCN (10 ml). After that, the same procedure than that of **9** was followed. Within 4 days colourless crystals grew on the test tube wall and green powder precipitated at the bottom. Crystallographic data verified colourless crystals were triethylamine hydrochloride ($\text{Et}_3\text{N} \cdot \text{HCl}$). $\text{Et}_3\text{N} \cdot \text{HCl}$ was easily removed and, to isolate the powder, solvent was removed via syringe and the residue was dried under vacuum. Some ml of Et_2O were used to clean the product, then it was removed via syringe and the product dried again under vacuum. IR spectroscopy was not enough to characterize green powder. The approximate yield was 11% assuming powder was the butterfly complex.

X-ray measurements were performed at 100 K in a XcaliburTM S X-ray Diffraction System from Rigaku Oxford Diffraction. The determination, visualization and analysis of molecular crystal structures were performed by using *Olex*² programme²³. Compounds **1**, **2** and **9** were solved by direct and Patterson methods (SHELEXS-97), and refined (SHELEXL-97) by full least matrix least-squares on all F^2 data.

Infrared measurements of all compounds were performed in a PerkinElmer Spectrum 100 FT-IR Spectrometer in the range of 4000-650 cm^{-1} .

7. Results and discussion

7.1 Butterfly $\{\text{Co}^{\text{III}}_2\text{Dy}^{\text{III}}_2\}$ complexes

$[\text{Co}^{\text{III}}_2\text{Dy}^{\text{III}}_2(\mu_3\text{-OMe})_2(\text{teaH})_2(\text{O}_2\text{CPh})_4(\text{MeOH})_2](\text{NO}_3)_2 \cdot \text{MeOH} \cdot \text{H}_2\text{O}$ (**1a**) and $[\text{Co}^{\text{III}}_2\text{Dy}^{\text{III}}_2(\mu_3\text{-OMe})_2(\text{teaH})_2(\text{O}_2\text{CPh})_4(\text{MeOH})_4](\text{NO}_3)_2 \cdot \text{MeOH} \cdot \text{H}_2\text{O}$ (**1b**)

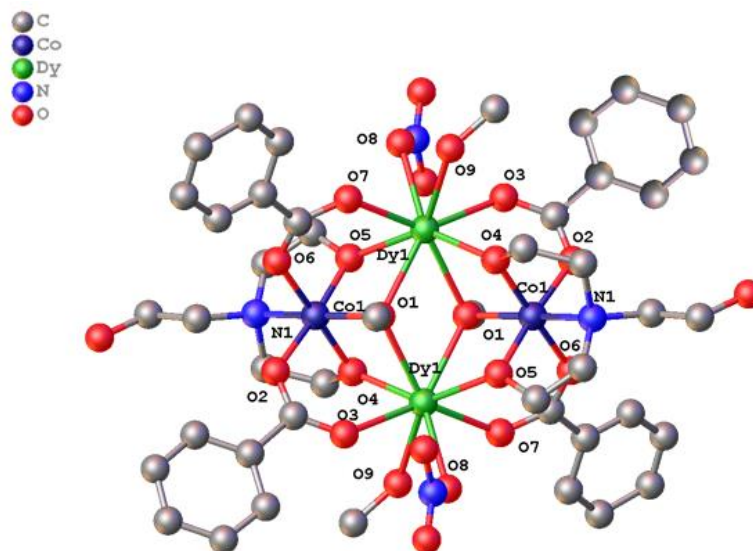


Figure 13. Structure of $[\text{Dy}^{\text{III}}_2\text{Co}^{\text{III}}_2(\text{OMe})_2(\text{teaH})_2(\text{O}_2\text{CPh})_4(\text{MeOH})_2(\text{NO}_3)_2] \cdot \text{MeOH} \cdot \text{H}_2\text{O}$ (**1a**). Solvent molecules and H atoms are omitted for clarity.

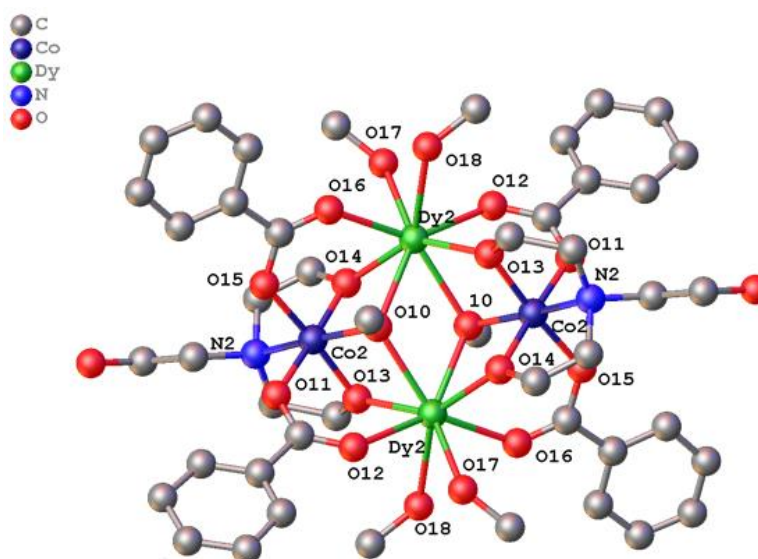


Figure 14. Structure of $[\text{Co}^{\text{III}}_2\text{Dy}^{\text{III}}_2(\mu_3\text{-OMe})_2(\text{teaH})_2(\text{O}_2\text{CPh})_4(\text{MeOH})_4](\text{NO}_3)_2 \cdot \text{MeOH} \cdot \text{H}_2\text{O}$ (**1b**). Solvent molecules, NO_3^- counterions and H atoms are omitted for clarity.

Crystal structure description

Complexes **1a** and **1b** are heterometallic tetranuclear complexes which cocrystallize in the tetragonal space group $I4_1/a$. **1a** is found to have one coordinated methanol and nitrate molecules coordinated to the Dy^{III} ion and a solvent MeOH molecule found in the lattice. **1b** has two MeOH molecules coordinated to the Dy^{III} site with a nitrate counterion in the lattice (Figures 13 and 14). Thus, **1a** is neutral and **1b** is cationic. For descriptive purposes **1a** and **1b** can be considered as equivalent and subsequently both will be described as compound **1**.

Table 3. Crystallographic data for compounds **1a** and **1b**.

Empirical formula^a	Co ₂ Dy ₂ C ₄₆ H ₇₀ N ₄ O ₂₇
Formula weight (g/mol)	1553.92
Data collection T (K)	150
Crystal system	tetragonal
Space group	$I4_1/a$
a (Å)	40.986(6)
b (Å)	40.986(6)
c (Å)	15.985(5)
α (°)	90
β (°)	90
γ (°)	90
Volume (Å³)	26852(9)
Z	16
ρ_{calc} (g/cm³)	1.535
Radiation	MoKα (λ = 0.71073 Å)

^aThe average formula of the two molecules is given, including solvate molecules.

Complex **1** consists of two Co^{III} and two Dy^{III} ions, with the metallic core best described as a planar butterfly motif, with the Dy^{III} ions occupying the body positions and the Co^{III} ions the outer wing-tips. The core is stabilized by two μ₃-methoxide ligands, both bridging to two Dy^{III} ions and one Co^{III} ion. Around the periphery of the cluster are four benzoate ligands bridging a Co^{III} to a Dy^{III} ion. There are also two doubly deprotonated teaH²⁻ ligands, with the N-atom coordinating to a wing-tip Co^{III} ion and the O-atoms bridging from the Co^{III} to the body Dy^{III} ions, with the protonated alcohol arm being non-coordinating. The two Co^{III} ions are six coordinate with octahedral geometries with an average Co-L_{N,O} bond length of 1.920 Å (**1a**), and 1.916 Å (**1b**). The two Dy^{III} ions are eight coordinate with distorted square antiprismatic geometries with an average Dy-O bond

length of 2.371 Å (**1a**), and 2.365 Å (**1b**). The intramolecular Dy...Dy distance is 4.088 Å (**1a**) and 4.075 Å (**1b**). **Tables 14** and **15** with Co-L_{O,N} and Dy-O bond lengths are found in the Annexes section.

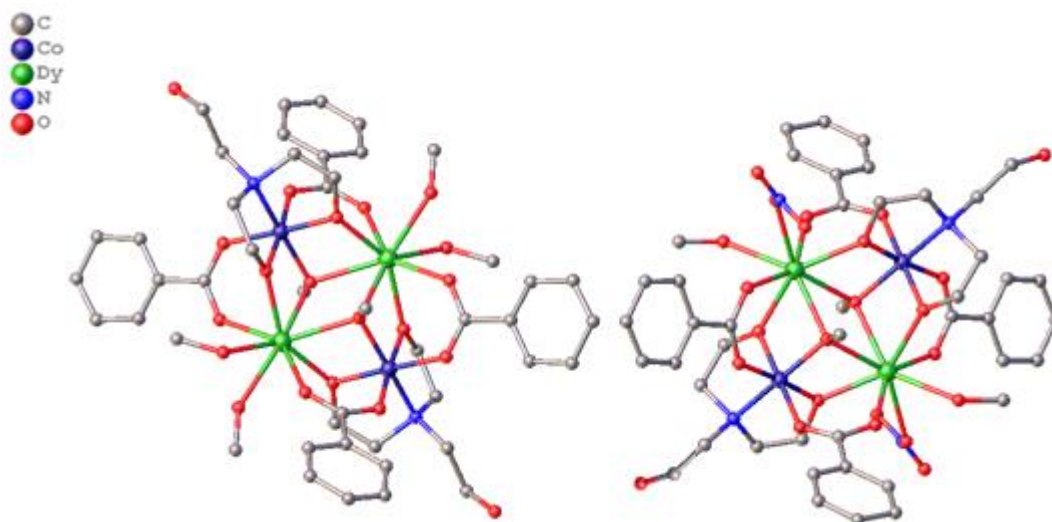


Figure 15. Structure of 1a (left) and 1b (right) in the crystal. Solvent molecules, NO₃⁻ counterions, and H atoms are omitted for clarity.

IR spectrum information

Stretching vibrations between the metallic centres and the donor atoms of the ligands ($\nu(\text{M-L}_{\text{N,O}})$) are not visualized in the spectra of compounds **1** to **10** due to the low-frequency vibrations they present; usually in the range of 600-300 cm⁻¹.^{24,25} Furthermore, peak assignment is difficult to carry out since main absorptions, which are due to bending and low frequency stretching vibrations of the ligands structures, are located in the fingerprint region.

Therefore, the IR spectrum of the already reported¹¹ compound **1** is used as a pattern to verify if the tetranuclear 3d/4f complexes which have not been able to grow as appropriate single crystals have been successfully synthesized

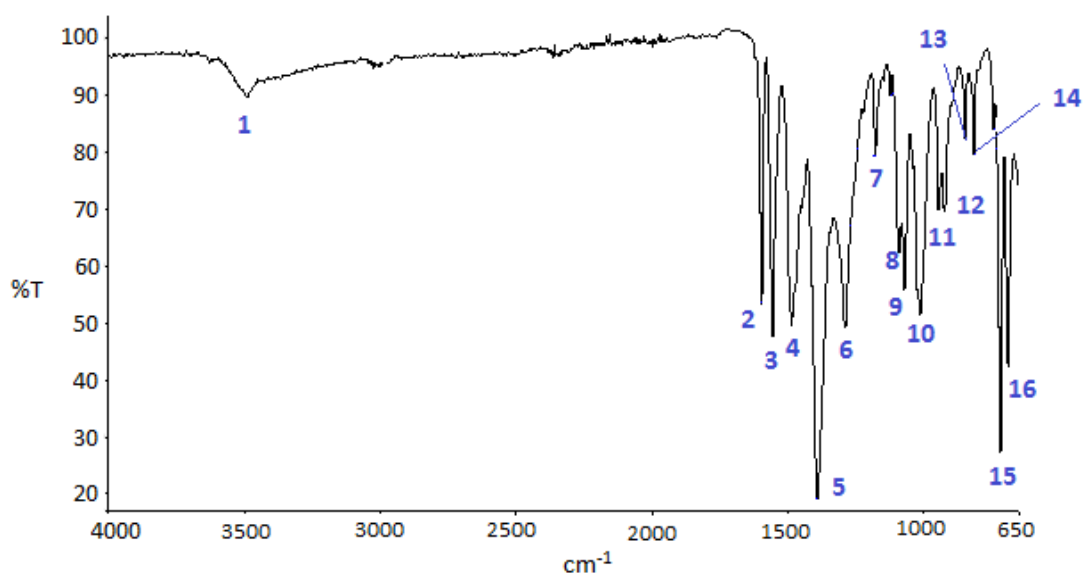


Figure 16. IR spectrum of compound 1.

Table 4. Selected IR data from compound 1.

Number	Wavenumber (cm ⁻¹)	Intensity	Number	Wavenumber (cm ⁻¹)	Intensity
1	3491	weak	9	1070	medium
2	1595	strong	10	1011	medium
3	1556	strong	11	944	weak
4	1485	strong	12	923	weak
5	1391	strong	13	847	weak
6	1288	medium	14	813	weak
7	1177	weak	15	715	strong
8	1089	medium	16	687	strong

Comments: peak number 1 corresponds to the stretching vibration $\nu(\text{O-H})$ of the hydroxyl group present in the ligand teaH^{2-} . Peaks present at approximately 1500 cm^{-1} or below are difficult to assign. Peak number 5 may correspond to bending vibrations of CH_2 groups present in the carbonated chains of the ligands.

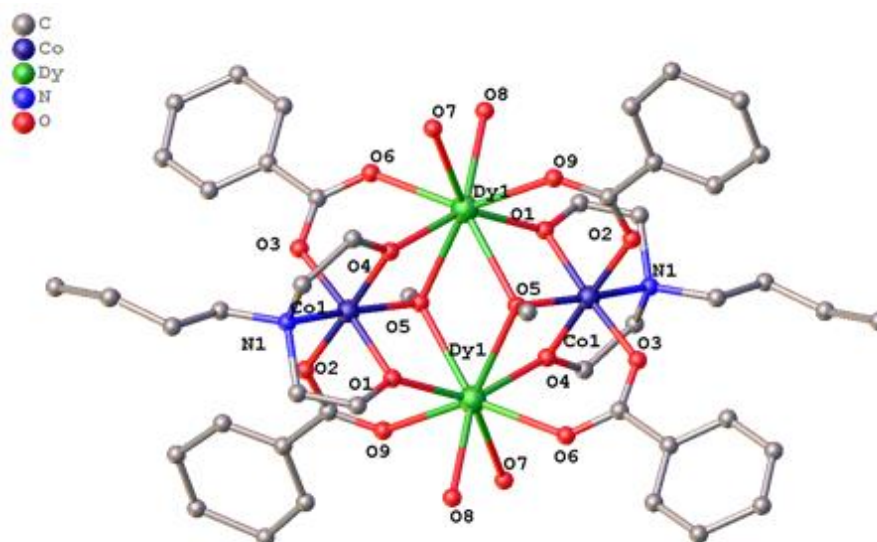
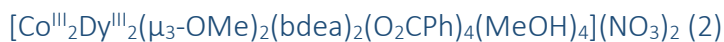


Figure 17. Structure of $[\text{Dy}^{\text{III}}_2\text{Co}^{\text{III}}_2(\text{OMe})_2(\text{bdea})_2(\text{O}_2\text{CPh})_4(\text{MeOH})_2(\text{NO}_3)_2]\cdot\text{MeOH}\cdot\text{H}_2\text{O}$ (**2**). H atoms are omitted for clarity.

Crystal structure description

Complex **2** (**Figure 17**) is an heterometallic tetranuclear complex which crystallizes in the monoclinic space group $P2_1/n$. Structurally, **2** is very similar to **1** in respect of the planar butterfly motif (Dy^{III} ions occupying the body positions and the Co^{III} ions the outer wing-tips) and the position and coordination of the peripheral ligands. In this complex, there are two doubly deprotonated bea²⁻ ligands instead of two teaH²⁻ ligands.

However, the data collected is not good enough to know all the ligands which are coordinated to the Dy^{III} ion because the obtained crystals were twinned. The data confirms the donor atom of the missing ligands is oxygen, but it is not possible to know if there are two methanol molecules, one methanol molecule and one nitrate molecule or, on the other hand, two cocrystallized products as in complex **1**.

The two Co^{III} ions are six coordinate with octahedral geometries with an average Co-L_{N,O} bond length of 1.912 Å. The two Dy^{III} ions are eight coordinate with distorted square antiprismatic geometries with an average Dy-O bond length of 2.379 Å. The intramolecular Dy...Dy distance is 4.067 Å. More detailed crystallographic data is found in **Table 5** and in **Table 16**, which is in the Annexes section, Dy-O and Co-L_{N,O} bond lengths are found.

Table 5. Crystallographic data for compound **2**.

Empirical formula	Co ₂ Dy ₂ C ₄₈ H ₇₄ N ₄ O ₂₅
Formula weight (g/mol)	1549.98
Data collection T (K)	150
Crystal system	monoclinic
Space group	P2 ₁ /n
a (Å)	7.9866(5)
b (Å)	23.2956(7)
c (Å)	17.6332(5)
α (°)	90
β (°)	90.414(4)
γ (°)	90
Volume (Å³)	3280.6(2)
Z	2
ρ_{calc} (g/cm³)	1.573
Radiation	MoKα (λ = 0.71073 Å)

IR spectrum information

IR spectra of compounds **2** to **10** are found in the Annexes section.

Table 6. Selected IR data from compound **2**. Selected peaks are those that compounds **1** and **2** have in common. Wavenumbers of complex **1** absorptions are in brackets to compare the data.

Number	Wavenumber (cm⁻¹)	Intensity	Number	Wavenumber (cm⁻¹)	Intensity
1	1596 (1595)	weak	8	1075 (1070)	medium
2	1559 (1556)	strong	9	1025 (1012)	medium
3	1478 (1485)	strong	10	848 (847)	weak
4	1395 (1391)	strong	11	815(813)	weak
5	1289 (1288)	strong	12	721 (715)	strong
6	1178 (1177)	medium	13	693 (687)	strong
7	1097 (1089)	weak			

Comments: peak around 3490 cm⁻¹ is not present because there are no hydroxyl groups in the complex. Peaks around 3000-2850 cm⁻¹ may correspond to CH₃ and CH₂ stretching

vibrations of some of the ligands. As it can be seen, the obtained IR spectrum is very similar to that of compound **1** due to the structural and chemical similarities.

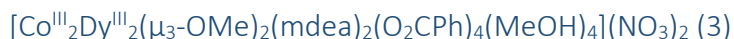


Table 7. Selected IR data from compound **3**. Selected peaks are those that compounds **1** and **3** have in common. Wavenumbers of complex **1** absorptions are in brackets to compare the data.

Number	Wavenumber (cm ⁻¹)	Intensity	Number	Wavenumber (cm ⁻¹)	Intensity
1	1597 (1595)	strong	6	1175 (1177)	weak
2	1558 (1556)	strong	7	1068 (1070)	strong
3	1445 (1485)	medium	8	1023 (1011)	strong
4	1382 (1391)	strong	9	718 (715)	strong
5	1312 (1288)	strong	10	684 (687)	medium

Comments: peak at 3386 cm⁻¹ is probably due to the presence of MeOH which was not removed properly when cleaning the product. This broad band corresponds to the $\nu(\text{O-H})$ of the H-bonded hydroxyl groups of MeOH. Furthermore, many peaks are broad when in other IR spectra these are sharper. This may be because the product contains some impurities, such as unreacted ligands and remaining solvent, which make other peaks appear and overlap those of interest.

Despite the presence of impurities, the IR spectrum is very similar to those of compound **1** and **2** and, even though the growth of single crystals was not achieved and a more accurate characterization of the product could not be carried out, there is enough evidence to affirm the butterfly complex was synthesized.

Optimization of the synthetic procedure must be carried out to obtain single crystals for further characterization.

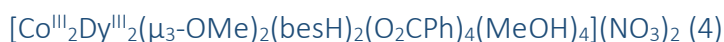


Table 8. Selected IR data from compound **4**. Selected peaks are those that compounds **1** and **4** have in common. Wavenumbers of complex **1** absorptions are in brackets to compare the data.

Number	Wavenumber (cm ⁻¹)	Intensity
1	1439 (1485)	weak
2	1402 (1391)	medium
3	1211 (1288)	strong
4	1067 (1176)	medium
5	717 (715)	strong

Comments: peak at 3453 cm⁻¹ is probably due to the presence of MeOH which was not removed properly when cleaning the product. The peak of weak intensity around 3000 cm⁻¹ may correspond to CH₃ and CH₂ stretching vibrations of some impurities such as unreacted ligands.

There are not many similar peaks to those of compound **1**. Furthermore, the wavenumbers of peaks differ more to those of compound **1** than in other complexes. This may happen because, in this case, the amino-polyalcohol present in this complex is chemically more different than those used before due to the presence of the sulfonic group. It could explain why the fingerprint region highly differs to that of the other complexes.

The IR spectrum is not as reliable as in previous complexes. Therefore, it cannot be affirmed with the same certainty the expected product has been synthesized successfully.

Optimization of the synthetic procedure must be carried out to obtain single crystals for further characterization.

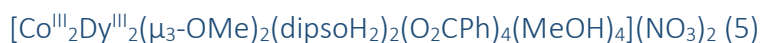


Table 9. Selected IR data from compound **5**. Selected peaks are those that compounds **1** and **5** have in common. Wavenumbers of complex **1** absorptions are in brackets to compare the data.

Number	Wavenumber (cm ⁻¹)	Intensity
1	1595 (1595)	strong
2	1557 (1556)	strong
3	1391 (1391)	strong
4	847 (847)	weak
5	813 (813)	weak
6	717 (715)	strong
7	687 (687)	medium

Comments: peak at 3380 cm⁻¹ is due to a stretching vibration $\nu(\text{O-H})$ of H-bonded hydroxyl groups. This can be originated because of the presence of MeOH which was not removed properly when cleaning the product or due to the presence in the product of non-deprotonated hydroxyl groups from DIPSO.

In contrast to compound **4**, which also contains an amino-polyalcohol ligand with a sulfonic group, IR spectrum of compound **5** presents more peaks that match with those of a butterfly complex. Selected peaks present wavenumbers and intensities practically identical to compound **1**, which provides evidences the butterfly complex is likely to have formed. Furthermore, peaks **a** and **b** are also present in the IR spectrum of compound **4**, which means these peaks may correspond to some bending vibration of the sulfonic acid ligand of the complex.

Optimization of the synthetic procedure must be carried out to obtain single crystals for further characterization.

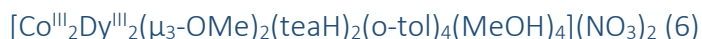


Table 10. Selected IR data from compound **6**. Selected peaks are those that compounds **1** and **6** have in common. Wavenumbers of complex **1** absorptions are in brackets to compare the data.

Number	Wavenumber (cm ⁻¹)	Intensity
1	1581 (1595)	medium
2	1559 (1556)	medium
3	1390 (1391)	strong
4	1301 (1288)	strong
5	1170 (1177)	weak

Comments: some peaks of the IR spectrum match to those of compound **1** as shown in **Table 10**. However, compound **6** could not be isolated due to the appearance of an oily residue when removing the solvent. As the product contains impurities of the reagents, some peaks are overlapped by other ones.

Even though the pattern shown in the IR spectrum seem to give evidence of the presence of the butterfly complex, optimization of the synthetic procedure must be carried out to avoid the appearance of the oily residue as well as the presence of impurities and obtain single crystals for further characterization.



Table 11. Selected IR data from compound **7**. Selected peaks are those that compounds **1** and **7** have in common. Wavenumbers of complex **1** absorptions are in brackets to compare the data.

Number	Wavenumber (cm ⁻¹)	Intensity	Number	Wavenumber (cm ⁻¹)	Intensity
1	1580 (1595)	medium	6	1155 (1177)	weak
2	1545 (1556)	medium	7	1096 (1090)	medium
3	1434 (1485)	medium	8	740 (715)	strong
4	1374 (1390)	strong	9	667 (687)	medium
5	1314 (1288)	strong			

Comments: the peak at 3380 cm⁻¹ corresponds to some MeOH which was not removed when cleaning the product. Many peaks of the IR spectrum match to those of compound **1** as shown in **Table 11**. However, compound **7** present several impurities as it is shown in the IR spectrum, where some peaks are overlapped.

The IR spectrum shows evidence of the presence of the butterfly complex. Optimization of the synthetic procedure must be carried out to avoid the presence of impurities and to obtain single crystals for further characterization.

7.2 Butterfly $\{V^{III}_2Dy^{III}_2\}$ complexes

Attempted $[V^{III}_2Dy^{III}_2(\mu_3-OMe)_2(teaH)_2(O_2CPh)_4(MeOH)_4](NO_3)_2$ (8)

One of the main problems of the synthesis of V^{III} complexes is the crystallization of important amounts of the by-product $Et_3N \cdot HCl$ when using $VCl_3 \cdot THF$ as source of V^{III} and Et_3N as base. Hence, the base was changed into $MeONa$ to avoid the appearance of the mentioned salt. However, the use of $MeONa$ as base instead of Et_3N led to the appearance of another by-product: triethanolamine hydrochloride ($teaH_4Cl$). It was known the new colourless crystals were triethanolamine hydrochloride because, once the crystal was analysed by X-Ray diffraction, a crystallographic database called *Conquest* was used to match the crystallographic data to the product.

An IR spectrum is found in the Annexes section. The spectrum obtained matches to the spectrum found in the literature for triethanolamine hydrochloride.²⁶ Main peaks are located at 3304 cm^{-1} , corresponding to $\nu(O-H)$, and 3158 cm^{-1} , corresponding to $\nu(N-H)$ of ammonium salts.²⁷

Therefore, optimization of the synthetic procedure must be carried out to avoid the appearance of by-products and to obtain single crystals for further characterization.

Attempted $[V^{III}_2Dy^{III}_2(\mu_3-OMe)_2(bdea)_2(O_2CPh)_4(MeOH)_4](NO_3)_2$ (9)

Once the obtained yellow crystals were analysed by single crystal X-ray diffraction, it was known the expected V^{III}/Dy^{III} butterfly complex was not synthesized. The product is a previously non-reported compound of chemical formula $Dy(O_2CPh)_3(MeOH)_2$ which forms chains. The crystal structure present two different Dy^{III} metallic centres where ligands coordinate spatially different, as shown in **Figure 18**. The chain structure of the complex is shown in **Figure 21**.

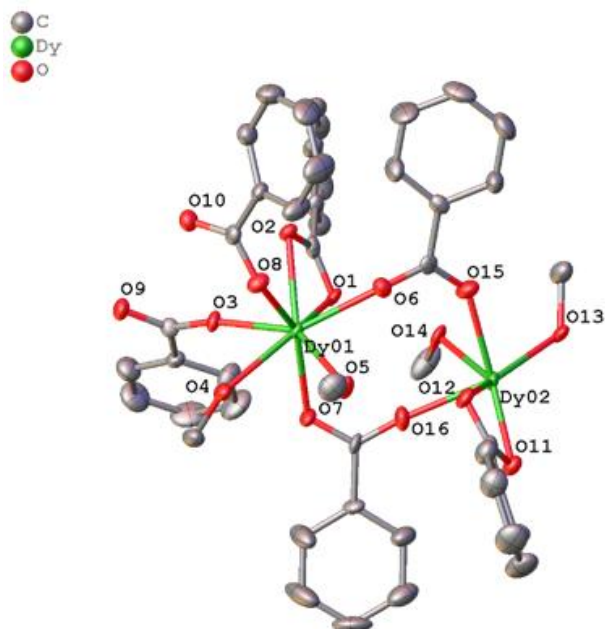


Figure 18. Asymmetric unit of $\text{Dy}(\text{O}_2\text{CPh})_3(\text{MeOH})_2$ complex.

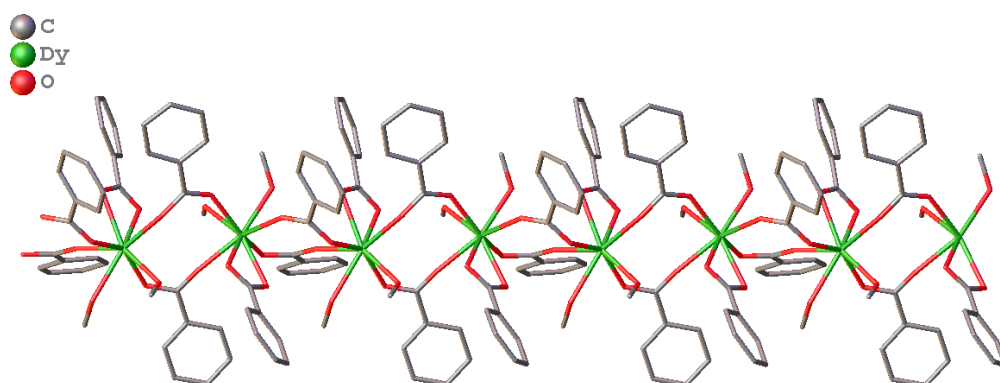


Figure 19. Chain structure of $\text{Dy}(\text{O}_2\text{CPh})_3(\text{MeOH})_2$ complex.

Crystal structure description

$\text{Dy}(\text{O}_2\text{CPh})_3(\text{MeOH})_2$ crystallizes in the monoclinic space group $P2_1/c$. In each Dy^{III} ion three types of ligands are coordinated: a chelating benzoate ligand, two methanol molecules and three bridging benzoates that connect two adjacent Dy^{III} ions.

Thus, each Dy^{III} ion is eight coordinate with distorted square antiprismatic geometry with an average Dy-O bond length of 2.441 Å. More detailed crystallographic data is found in **Table 12** and in **Table 17**, which is in the Annexes section, Dy-O bond lengths are found.

Table 12. Crystallographic data for compound **9**.

Empirical formula	C ₂₃ H ₂₃ DyO ₈
Formula weight (g/mol)	589.91
Data collection temperature (K)	150
Crystal system	monoclinic
Space group	P2 ₁ /c
a (Å)	9.6279(3)
b (Å)	21.4484(5)
c (Å)	21.9893(7)
α (°)	90
β (°)	90.799(3)
γ (°)	90
Volume (Å³)	4540.4(2)
Z	8
ρ_{calc} (g/cm³)	1.726
Radiation	MoKα (λ = 0.71073nm)

IR spectrum information

The IR spectrum shows clearly two strong peaks at 1523 cm⁻¹ (peak **1**) and 1396 cm⁻¹ (peak **2**). These peaks correspond, respectively, to the asymmetric and symmetric $\nu(\text{C}-\text{O})$ of the benzoate ligands present in the complex.

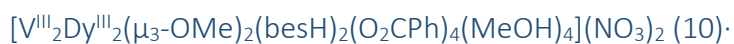


Table 13. Selected IR data from compound **10**. Selected peaks are those that compounds **1** and **10** have in common. Wavenumbers of complex **1** absorptions are in brackets to compare the data.

Number	Wavenumber (cm ⁻¹)	Intensity
1	1598 (1595)	weak
2	1547 (1556)	weak
3	1474 (1485)	weak
4	1404 (1390)	medium

Comments: Some peaks of the IR spectrum match to those of compound **1** as shown in **Table 10**. However, the intensity of these peaks is weak while in the spectrum of compound **1** their intensity is higher. Furthermore, more intense peaks appear below 1400 and overlap each other. This may show evidence of the presence of many impurities or another complex has been synthesized.

As not much information can be provided by the IR spectrum, the synthesis of this V^{III}/Dy^{III} butterfly complex cannot be verified. Therefore, optimization of the synthetic procedure must be carried out to obtain single crystals for further characterization.

8. Conclusions

New $\{\text{Co}^{\text{III}}_2\text{Dy}^{\text{III}}_2\}$ and $\{\text{V}^{\text{III}}_2\text{Dy}^{\text{III}}_2\}$ tetranuclear complexes have been tried to synthesize utilizing amino-polyalcohols and carboxylic acids as bridging ligands.

As for $\{\text{Co}^{\text{III}}_2\text{Dy}^{\text{III}}_2\}$ complexes, $[\text{Co}^{\text{III}}_2\text{Dy}^{\text{III}}_2(\mu_3\text{-OMe})_2(\text{bdea})_2(\text{O}_2\text{CPh})_4(\text{MeOH})_4](\text{NO}_3)_2$ is the only complex which has been able to crystallize, providing single crystals which can be characterized by single crystal X-ray diffraction. However, crystals are twinned and their quality is not high enough for complete characterisation. For the analogue complexes which contain MDEA, DIPSO and BES instead of BDEA, microcrystalline powder has been obtained. Nevertheless, IR data verifies the compounds may have been successfully synthesized because of the high matching of peaks when comparing to the IR data of a reported $\{\text{Co}_2\text{Dy}_2\}$ butterfly complex. Finally, IR data also confirms the synthesis of $[\text{Co}^{\text{III}}_2\text{Dy}^{\text{III}}_2(\mu_3\text{-OMe})_2(\text{teaH})_2(\text{o-tol})_4(\text{MeOH})_4](\text{NO}_3)_2$ and $[\text{Co}^{\text{III}}_2\text{Dy}^{\text{III}}_2(\mu_3\text{-OMe})_2(\text{teaH})_2(\text{O}_2\text{CPh-2-Cl})_4(\text{MeOH})_4](\text{NO}_3)_2$ but they have not been able to be isolated from impurities.

As for $\{\text{V}^{\text{III}}_2\text{Dy}^{\text{III}}_2\}$ complexes, none of the expected products have been obtained. The main issue is the appearance of by-products such as triethylamine and triethanolamine hydrochlorides. Furthermore, an unexpected and non-reported coordination complex was obtained, $\text{Dy}(\text{O}_2\text{CPh})_3(\text{MeOH})_2$, when trying to synthesize a $\{\text{V}^{\text{III}}_2\text{Dy}^{\text{III}}_2\}$ butterfly complex using triethanolamine and benzoic acid as ligands.

In summary, further research must be carried out to optimize the synthetic procedures to obtain single crystals for further characterization and to avoid the presence of by-products. Moreover, IR data cannot provide enough information to know the combinations of MeOH and NO_3^{2-} ligands coordinated to Dy^{III} ions. With regard to $\{\text{Co}^{\text{III}}_2\text{Dy}^{\text{III}}_2\}$ complexes, the utilization of slower crystal growth techniques as vapour diffusion may improve the crystallization process as well as finding more appropriate solvents. As for $\{\text{V}^{\text{III}}_2\text{Dy}^{\text{III}}_2\}$ complexes, finding more appropriate solvents, not using amines as base and non-chlorinated V^{III} sources should avoid the crystallization of chlorinated salts and lead to single crystals.

9. References

- (1) Feltham, H. L. C.; Brooker, S. *Coord. Chem. Rev.* **2014**, *276*, 1–33.
- (2) Sadler, M. Inside a Magnet - ACA Grade 8 Science <http://acamrmicheal.weebly.com/magnets-domains.html> (accessed May 27, 2017).
- (3) Woodruff, D. N.; Winpenny, R. E. P.; Layfield, R. A. *Chem. Rev.* **2013**, *113* (7), 5110–5148.
- (4) Vignesh, K. R.; Langley, S. K.; Murray, K. S.; Rajaraman, G. *Inorg. Chem.* **2017**, *56* (5), 2518–2532.
- (5) Winpenny, R. E. P.; McInnes, E. J. L. In *Molecular Materials*; John Wiley & Sons, Ltd: Chichester, UK, 2010; pp 283, 285.
- (6) Cornia, A.; Mannini, M.; Sainctavit, P.; Sessoli, R. *Chem. Soc. Rev.* **2011**, *40* (6), 3076–3091.
- (7) Zhou, C.-L.; Wang, Z.-M.; Wang, B.-W.; Gao, S. *Polyhedron* **2011**, *30* (18), 3279–3283.
- (8) Freedman, D. E.; Harman, W. H.; Harris, T. D.; Long, G. J.; Chang, C. J.; Long, J. R. *J. Am. Chem. Soc.* **2010**, *132* (4), 1224–1225.
- (9) Zadrozny, J. M.; Long, J. R. *J. Am. Chem. Soc.* **2011**, *133* (51), 20732–20734.
- (10) Zhang, P.; Guo, Y. N.; Tang, J. *Coord. Chem. Rev.* **2013**, *257* (11–12), 1728–1763.
- (11) Langley, S. K.; Chilton, N. F.; Ungur, L.; Moubaraki, B.; Chibotaru, L. F.; Murray, K. S. *Inorg. Chem.* **2012**, *51* (21), 11873–11881.
- (12) Langley, S. K.; Le, C.; Ungur, L.; Moubaraki, B.; Abrahams, B. F.; Chibotaru, L. F.; Murray, K. S. *Inorg. Chem.* **2015**, *54* (7), 3631–3642.
- (13) Langley, S. K.; Chilton, N. F.; Ungur, L.; Moubaraki, B.; Chibotaru, L. F.; Murray, K. S. *Inorg. Chem.* **2012**, *51* (21), 11873–11881.
- (14) Craig, G. A.; Murrie, M. *Chem. Soc. Rev.* **2015**, *44* (8), 2135–2147.

- (15) Rajaraman, G. Molecular Modelling Group
<http://www.chem.iitb.ac.in/~rajaraman/mnms.html> (accessed Jun 7, 2017).
- (16) Gatteschi, D.; Sessoli, R.; Villain, J. *Molecular Nanomagnets*; Oxford University Press: New York, 2006.
- (17) Rinehart, J. D.; Fang, M.; Evans, W. J.; Long, J. R. *Nat Chem* **2011**, 3 (7), 538–542.
- (18) Millar, S. Tips and Tricks for the Lab: Growing Crystals Part 1
http://www.chemistryviews.org/details/education/2532131/Tips_and_Tricks_for_the_Lab_Growing_Crystals_Part_1.html (accessed May 19, 2017).
- (19) Our Facilities :: Faculty Of Science :: The University of Jordan
<http://science.ju.edu.jo/Lists/SciFacilities/Facilities.aspx> (accessed May 16, 2017).
- (20) Blake, A. J. Crystal Growth, Evaluation and Handling
<http://www.ccp14.ac.uk/ccp/web-mirrors/blake/~pczajb2/growcrys.htm.orig>
(accessed May 19, 2017).
- (21) Millar, S. Tips and Tricks for the Lab: Growing Crystals Part 2
http://www.chemistryviews.org/details/education/2345141/Tips_and_Tricks_for_the_Lab_Column_Troubleshooting_and_Alternatives.html (accessed May 19, 2017).
- (22) Millar, S. Tips and Tricks for the Lab: Growing Crystals Part 3
http://www.chemistryviews.org/details/education/2538941/Tips_and_Tricks_for_the_Lab_Growing_Crystals_Part_3.html (accessed Mar 30, 2017).
- (23) Dolomanov, O. V.; Bourhis, L. J.; Gildea, R. J.; Howard, J. A. K.; Puschmann, H.; IUCr; L., W.; G., P.; R., S. *J. Appl. Crystallogr.* **2009**, 42 (2), 339–341.
- (24) Nakamoto, K. In *Infrared and Raman Spectra of Inorganic and Coordination Compounds*; John Wiley & Sons, Inc.: Hoboken, NJ, USA, 2009; pp 64, 271.
- (25) Basile, L. J. In *Low-Frequency Vibrations of Inorganic and Coordination Compounds*; Springer US: Boston, MA, 1971; p 197.

- (26) Triethanolamine hydrochloride IR spectrum - National Institute of Standards and Technology <http://webbook.nist.gov/cgi/formula?ID=C637398&Mask=80#IR-Spec> (accessed Jun 5, 2017).
- (27) Heacock, R. A.; Marion, L. *Can. J. Chem.* **1956**, *34* (12), 1782–1795.

10. Annexes

[Co^{III}₂Dy^{III}₂(μ₃-OMe)₂(teaH)₂(O₂CPh)₄(MeOH)₂](NO₃)₂·MeOH·H₂O (1a) and
 [Co^{III}₂Dy^{III}₂(μ₃-OMe)₂(teaH)₂(O₂CPh)₄(MeOH)₄](NO₃)₂·MeOH·H₂O (1b)

Table 14. Co-L_{O,N} and Dy-O bond lengths of compound **1a**.

Bond	Bond length (Å)	Bond	Bond length (Å)
Co ₁ -O ₁	1.952(6)	Dy ₁ -O ₄	2.322(6)
Co ₁ -O ₂	1.905(6)	Dy ₁ -O ₅	2.245(6)
Co ₁ -O ₃	1.876(7)	Dy ₁ -O ₆	2.412(7)
Co ₁ -O ₄	1.896(6)	Dy ₁ -O ₇	2.456(7)
Co ₁ -O ₅	1.952(6)	Dy ₁ -O ₈	2.480(6)
Co ₁ -N ₁	1.964(7)	Dy ₁ -O ₉	2.479(7)
Dy ₁ -O ₁	2.235(7)		

Table 15. Co-L_{O,N} and Dy-O bond lengths of compound **1b**.

Bond	Bond length (Å)	Bond	Bond length (Å)
Co ₂ -O ₁₀	1.929(6)	Dy ₂ -O ₁₂	2.324(7)
Co ₂ -O ₁₁	1.896(7)	Dy ₂ -O ₁₃	2.428(6)
Co ₂ -O ₁₃	1.924(7)	Dy ₂ -O ₁₄	2.422(8)
Co ₂ -O ₁₄	1.891(7)	Dy ₂ -O ₁₆	2.441(7)
Co ₂ -O ₁₅	1.929(6)	Dy ₂ -O ₁₇	2.441(7)
Co ₂ -N ₂	1.964(8)	Dy ₂ -O ₁₈	2.448(6)
Dy ₂ -O ₁₀	2.207(1)		

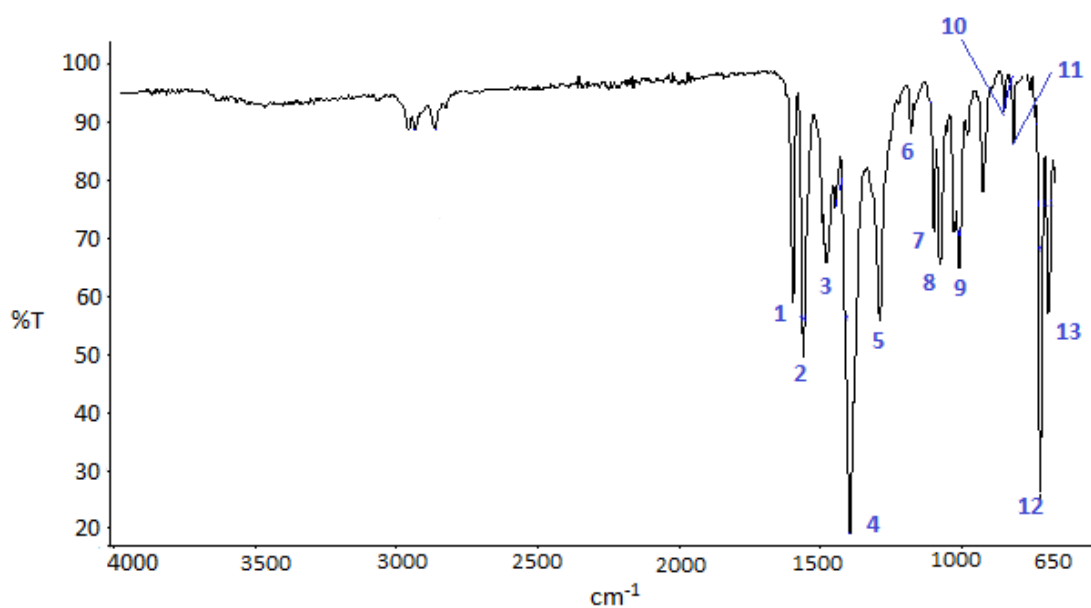
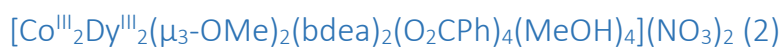


Figure 20. IR spectrum of compound **2**.

Table 16. Co- O_{N} and Dy-O bond lengths of compound **2**.

Bond	Bond length (Å)	Bond	Bond length (Å)
Co ₁ -O ₁	1.890(2)	Dy ₁ -O ₄	2.237(1)
Co ₁ -O ₂	1.909(1)	Dy ₁ -O ₅	2.418(1)
Co ₁ -O ₃	1.923(1)	Dy ₁ -O ₆	2.346(1)
Co ₁ -O ₄	1.886(4)	Dy ₁ -O ₇	2.570(3)
Co ₁ -O ₅	1.957(1)	Dy ₁ -O ₈	2.520(3)
Co ₁ -N ₁	1.908(2)	Dy ₁ -O ₉	2.356(1)
Dy ₁ -O ₁	2.207(1)		

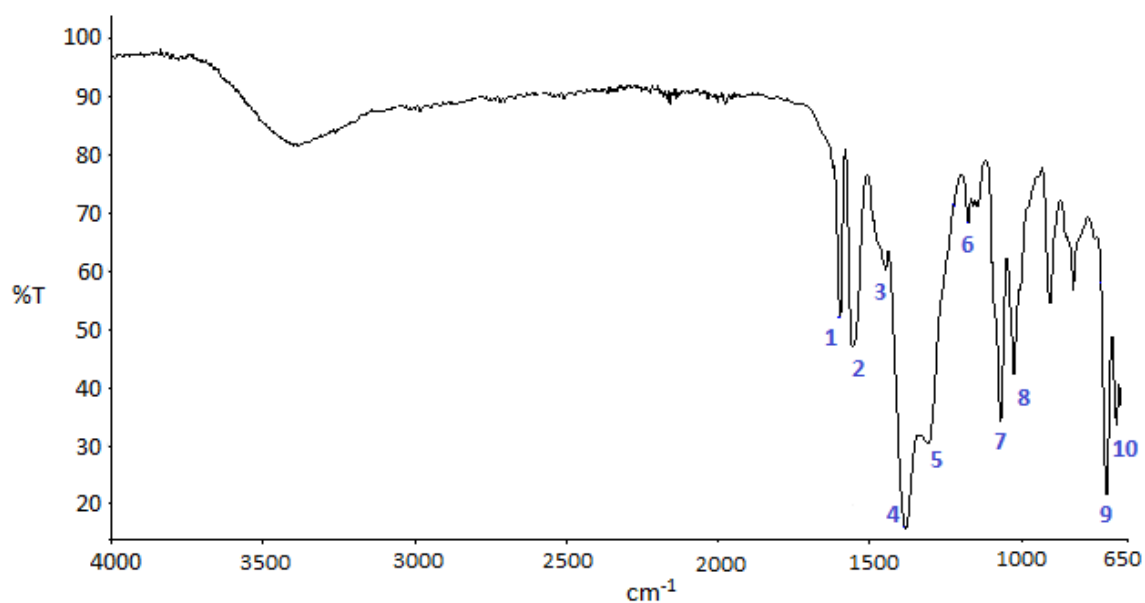
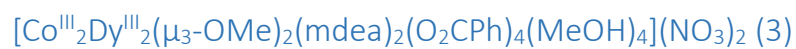


Figure 21. IR spectrum of compound 3.

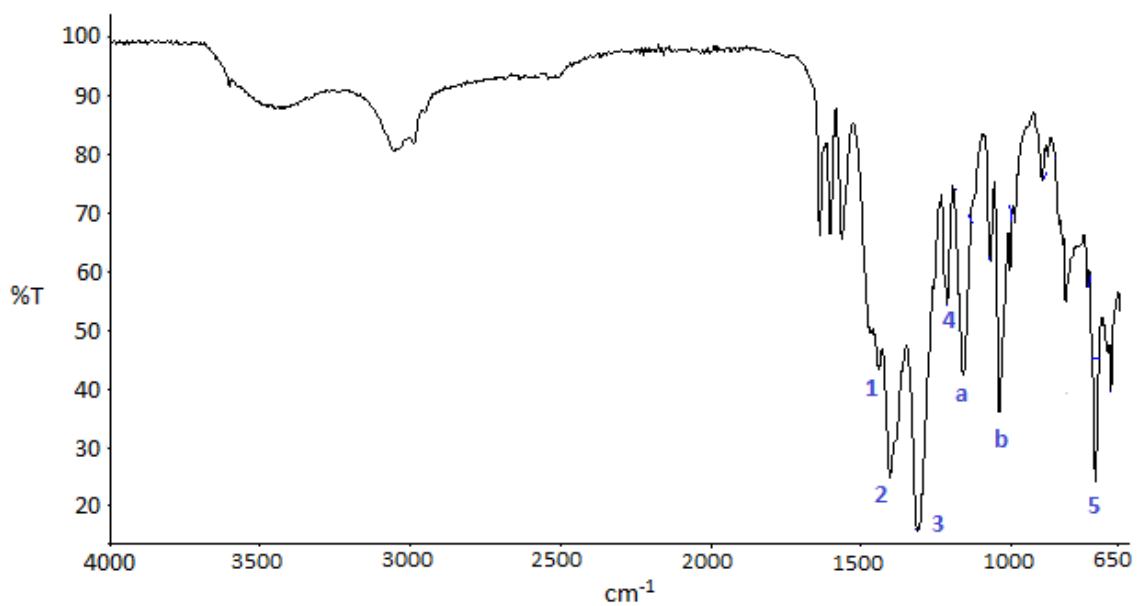
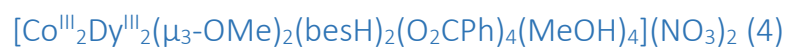


Figure 22. IR spectrum of compound 4.

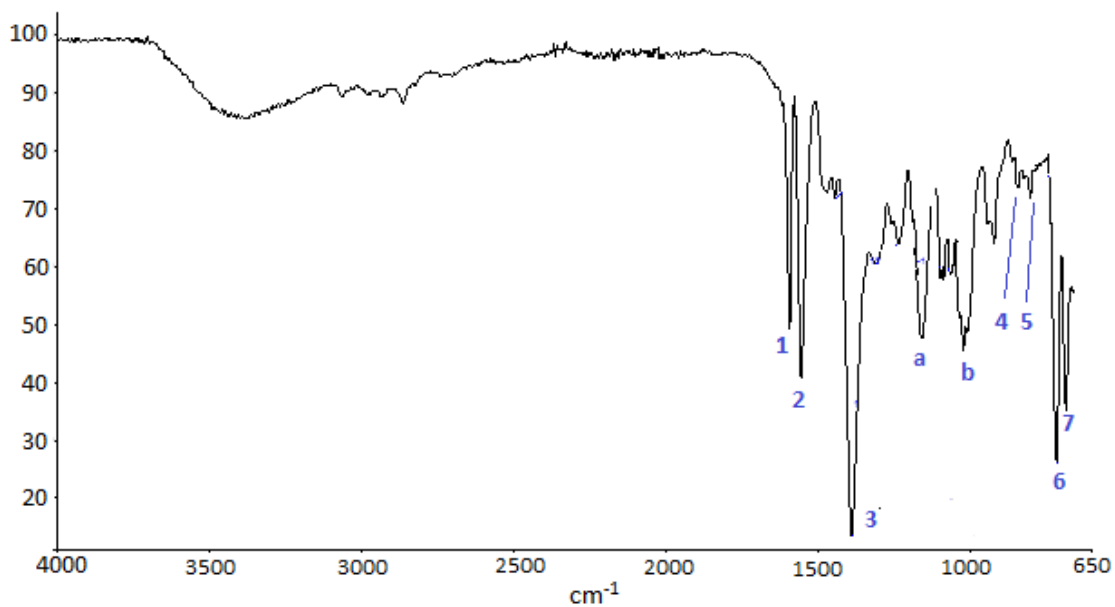
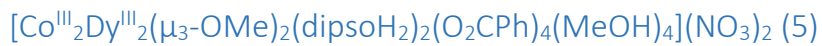


Figure 23. IR spectrum of compound 5.

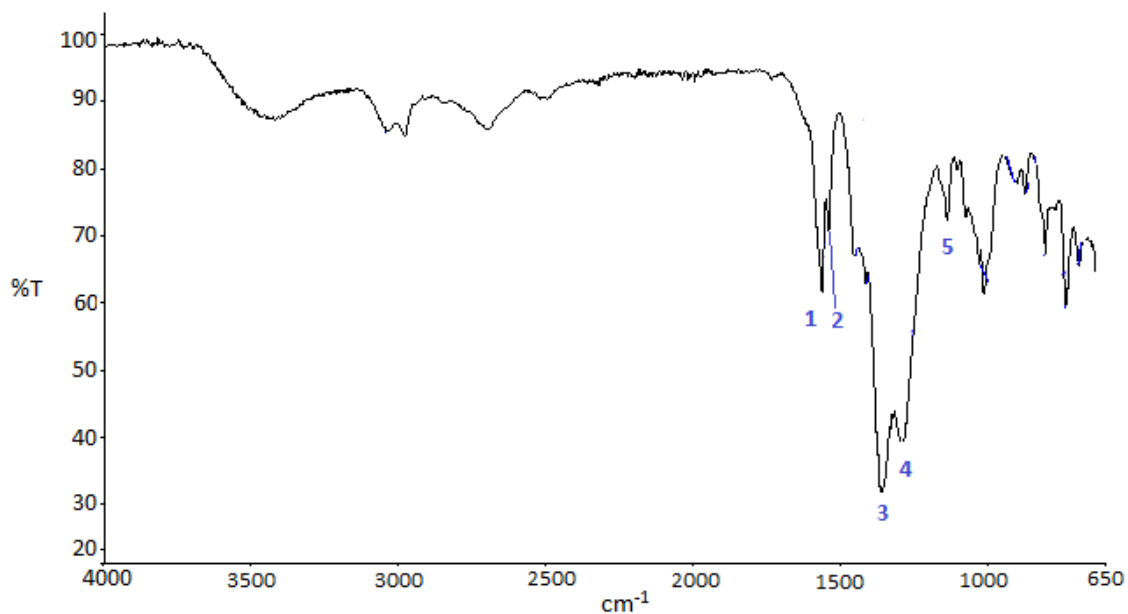
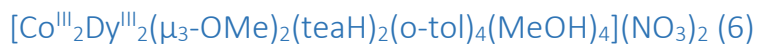


Figure 24. IR spectrum of compound 6.

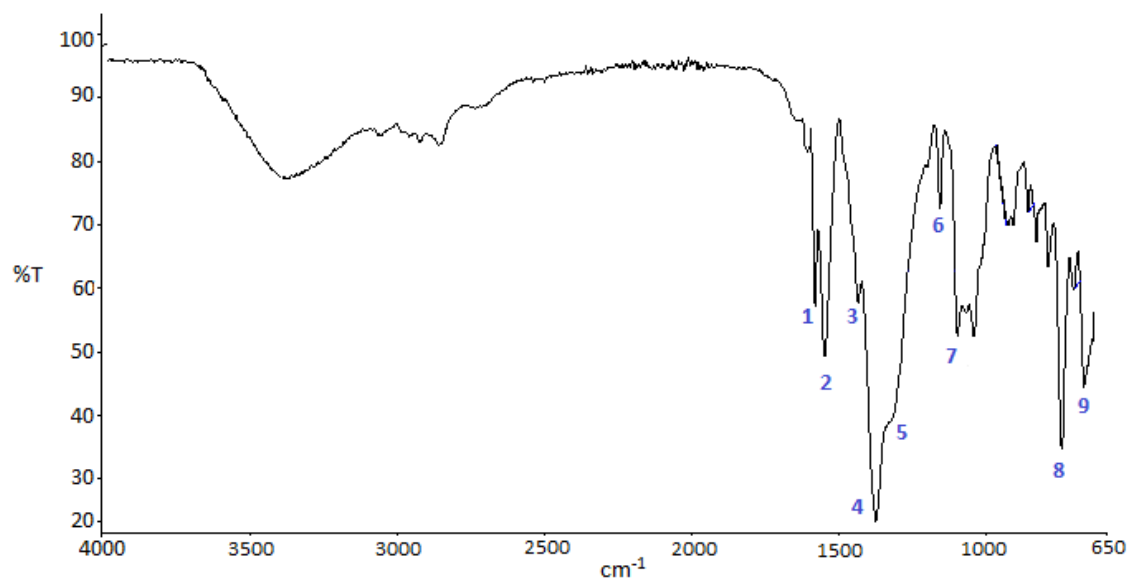


Figure 25. IR spectrum of compound 7.

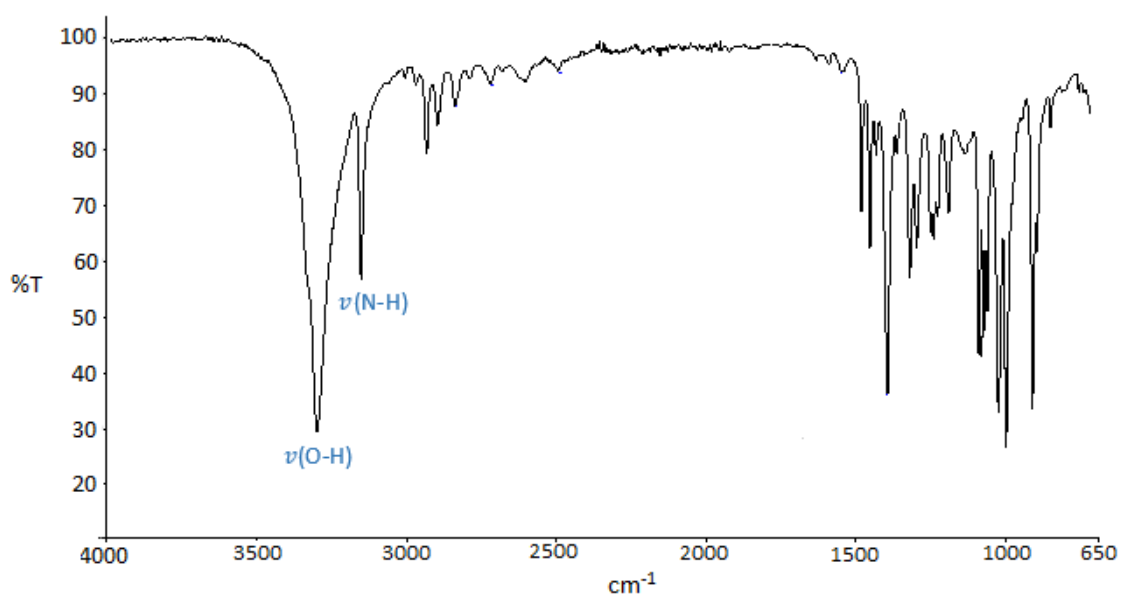


Figure 26. IR spectrum of (teaH₄)Cl (attempted compound 8).

Attempted $[\text{V}^{\text{III}}_2\text{Dy}^{\text{III}}_2(\mu_3\text{-OMe})_2(\text{bdea})_2(\text{O}_2\text{CPh})_4(\text{MeOH})_4](\text{NO}_3)_2$ (9)

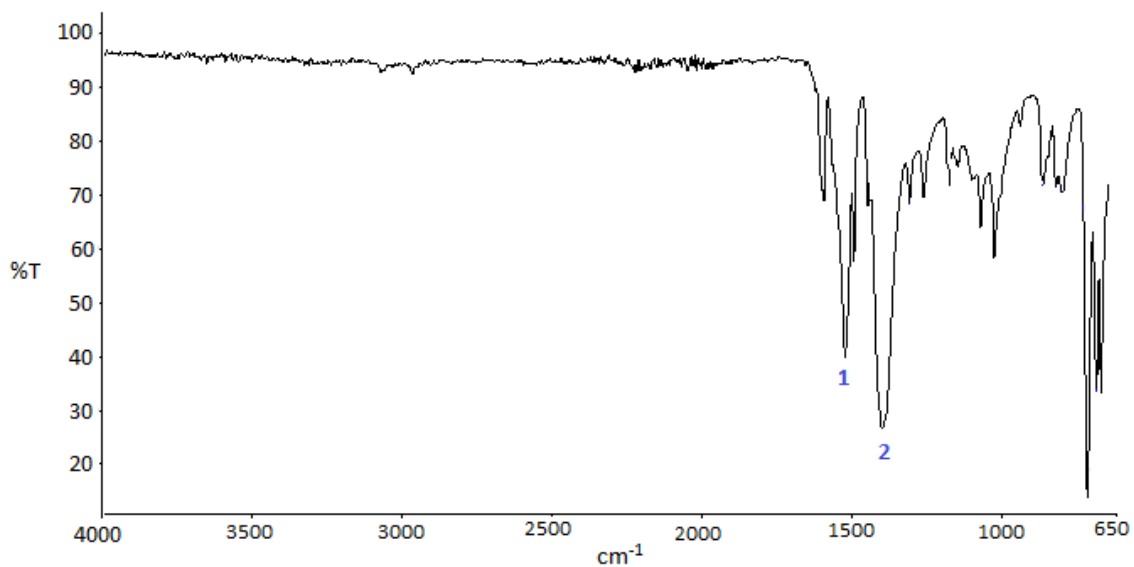


Figure 27. IR spectrum of $\text{Dy}(\text{O}_2\text{CPh})_3(\text{MeOH})_2$ (attempted compound 9).

Table 17. Dy-O bond lengths of attempted compound $\text{Dy}(\text{O}_2\text{CPh})_3(\text{MeOH})_2$ (attempted compound 9)

Bond	Bond length (Å)	Bond	Bond length (Å)
Dy ₁ -O ₁	2.433(4)	Dy ₂ -O ₉	2.316(5)
Dy ₁ -O ₂	2.480(5)	Dy ₂ -O ₁₀	2.312(4)
Dy ₁ -O ₃	2.297(4)	Dy ₂ -O ₁₁	2.425(5)
Dy ₁ -O ₄	2.467(4)	Dy ₂ -O ₁₂	2.495(5)
Dy ₁ -O ₅	2.448(5)	Dy ₂ -O ₁₃	2.448(4)
Dy ₁ -O ₆	2.291(4)	Dy ₂ -O ₁₄	2.496(5)
Dy ₁ -O ₇	2.301(5)	Dy ₂ -O ₁₅	2.290(5)
Dy ₁ -O ₈	2.268(5)	Dy ₂ -O ₁₆	2.278(4)

Attempted $[V^{III}_2Dy^{III}_2(\mu_3-OMe)_2(besH)_2(O_2CPh)_4(MeOH)_4](NO_3)_2 \cdot (10)$

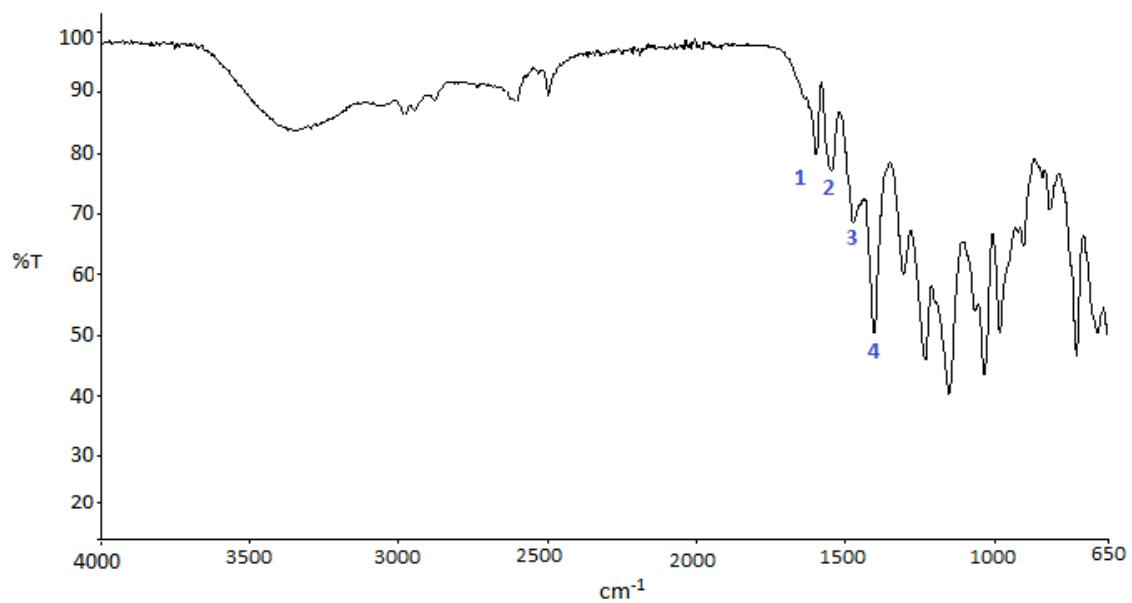


Figure 28. IR spectrum of attempted compound **10**.